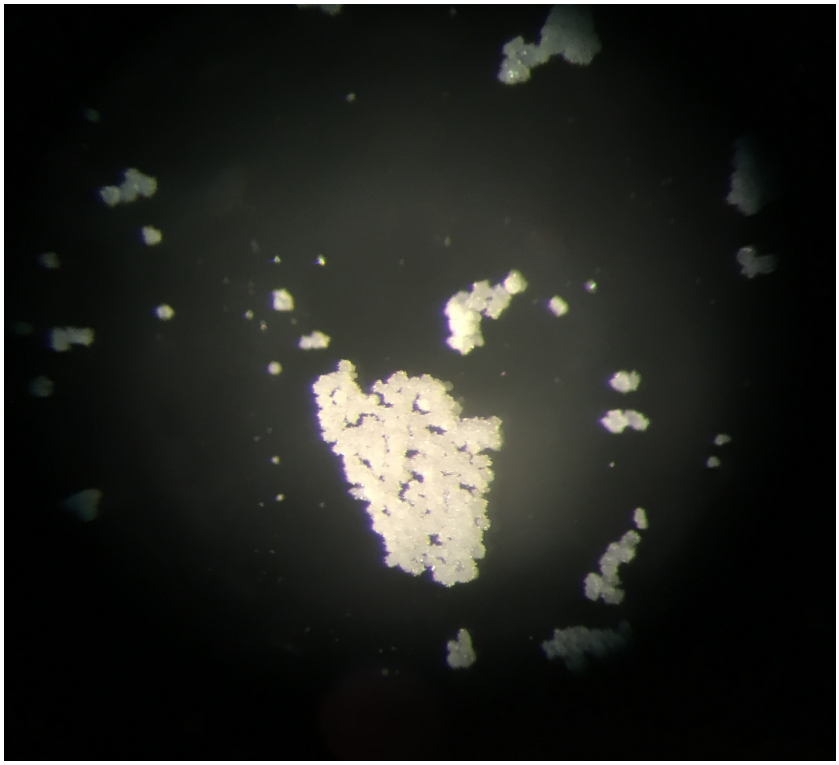
CHALMERS
UNIVERSITY OF TECHNOLOGY



Synthesis and development of hexagon-based metal-organic framework

Master's thesis in Materials Chemistry

Axel Jonsson

Department of Chemistry and Chemical Engineering
CHALMERS UNIVERSITY OF TECHNOLOGY
Gothenburg, Sweden 2020

Master's thesis 2020

Synthesis and development of hexagon-based metal-organic framework

AXEL JONSSON



CHALMERS
UNIVERSITY OF TECHNOLOGY

Department of Chemistry and Chemical Engineering
Chalmers University of Technology
Gothenburg, Sweden 2020

Synthesis and Development of Hexagon-Based Metal-Organic Framework
Axel Jonsson

© Axel Jonsson, 2020.

Supervisor: Lars Öhrström, Division of Chemistry and Biochemistry
Examiner: Jerker Mårtensson, Division of Chemistry and Biochemistry

Master's Thesis 2020:
Department of Chemistry and Chemical Engineering
Chalmers University of Technology
SE-412 96 Gothenburg
Telephone +46 31 772 1000

Cover: Magnesium crystals formed by hexagon shaped linker and magnesium nitrate from synthesis in Section. 4.1 seen in a Zeiss microscope.

Gothenburg, Sweden 2020

Synthesis and Development of Hexagon-Based Metal-Organic Framework
Axel Jonsson
Department of Chemistry and Chemical Engineering
Chalmers University of Technology

Abstract

The purpose of the project was to explore the possibilities of producing hexagon-based Metal-Organic Frameworks (MOFs) with the goal of synthesizing a new MOF structure through solvothermal synthesis. MOFs are often porous crystalline materials constructed from metal clusters connected with multidentate organic linkers to form a highly ordered network. Net structures of MOFs can be divided into the different basic geometrical topologies that their network form. Hexagon-based structures are less commonly reported than other geometrical shapes, this means that there are MOFs and topologies which are not yet explored.

Solvothermal synthesis of 22 samples were made with the organic linker 1',2',3',4',5',6'-hexakis(4-carboxyphenyl)benzene (H_6cpb) and metal ions such as europium, dysprosium, lanthanum, magnesium, indium, yttrium, chromium. Where the samples which produced precipitate was characterized through Powder X-ray Diffraction (PXRD), Thermogravimetric Analysis (TGA) and Fourier Transform Infrared Spectroscopy (FTIR). From these results several samples were crystalline and could potentially be new MOFs. A specific lanthanum sample would show a very distinct PXRD pattern and the structure could later solved through Transmission Electron Microscope (TEM). The preliminary results for this crystal would show that a new hexagon-based MOF with the chiral space group P/6 2 2 had been formed. This new MOF will be called CTH-17.

Keywords: MOFs, hexagon, reticular chemistry, solvothermal synthesis, CTH-17, SAXS, PXRD.

Acknowledgements

I would first like to thank Professor Lars Öhrström and Dr. Francoise Noa for their expertise in the field of Metal-organic frameworks and for the opportunity to work on this project. Further I would like to thank Victor Engdahl for his company in this project while working on his own parallel project. I would also like to thank Dr. Michal Strach at Chalmers Materials Analysis Laboratory for all the help and expertise with the PXRD and SAXS machine. I would also like to thank Dr. Francoise Noa and Mr. Erik Svensson Grape for the preliminary structure of CTH-17.

Axel Jonsson, Gothenburg, August 2020

Contents

List of Figures viii

List of Tables x

List of Abbreviations xi

1 Introduction 1
- 1.1 Aim . . . 1
- 1.2 Limitations . . . 2
- 1.3 Specification of issue under investigation . . . 2

2 Theory 3
- 2.1 Reticular chemistry . . . 3
- 2.2 Metals . . . 3
  - 2.2.1 Alkaline earth metals . . . 3
  - 2.2.2 Chromium . . . 4
  - 2.2.3 Lanthanoids . . . 4
  - 2.2.4 Yttrium . . . 4
  - 2.2.5 Indium . . . 4
- 2.3 Linkers . . . 4
- 2.4 Characteristics . . . 5
- 2.5 Solvothermal synthesis . . . 7
- 2.6 Modes of analysis . . . 7
  - 2.6.1 Crystal diffraction analysis . . . 7
  - 2.6.2 Fourier Transform Infrared Spectroscopy . . . 8
  - 2.6.3 Thermogravimetric analysis . . . 9
- 2.7 Potential applications . . . 9
  - 2.7.1 I_2-sorption . . . 9
  - 2.7.2 CO_2-sorption . . . 9
  - 2.7.3 Solar Cells . . . 9

3 Methodology 10
- 3.1 Synthesis of MOFs . . . 10
- 3.2 Filtration . . . 10
- 3.3 Drying . . . 11
- 3.4 Methods for characterization . . . 11
- 3.5 Thermogravimetric analysis . . . 11
- 3.6 Fourier Transform Infrared Spectroscopy . . . 11
- 3.7 PXRD through SAXS . . . 11

3.7.1 Capillaries 12
3.7.2 Transparent adhesive tape method 12

4 Experimental **13**
4.1 Synthesis with hexatopic H_6cpb 13
4.2 High temperature synthesis with hexatopic H_6cpb 13
4.3 Synthesis of MOF-889 14
4.4 Synthesis using H_6cpb & ppb 14
4.5 Synthesis of lanthanum and indium with H_6cpb 15

5 Results and Discussion **16**
5.1 Synthesis with hexatopic H_6cpb 16
5.2 High temperature synthesis with hexatopic H_6CPB 16
5.3 Result from synthesis of MOF-889 17
5.4 Results from synthesis using H_6cpb & ppb 17
5.5 Results from synthesis of lanthanum and indium with H_6cpb 19
5.6 IR results 19
5.7 TGA results 22
5.8 PXRD results 23
5.9 UV-test 28
5.10 TEM results 29

6 Conclusion **31**

Bibliography **32**

Appendix **i**

List of Figures

2.1 The hexatopic organic linkers called H_6cpb and H_6ppb 5
2.2 Trigonal (3-c) in **green** and hexagonal (6-c) in **red** are the building units to build the **kgd** net. 6
2.3 The **laf** net in the image to the **left**. The same configuration when folded to the **right**. 6
2.4 Trigonal bipyramid (5-c) in **green** and hexagonal (6-c) in **red** are the building units to build the **yav**. 7

5.1 PXRD measurement of Nickel sample from synthesis in Section 4.4 in **blue**, this has been plotted with a diffraction pattern of H_6cpb without any constituents in **green**. 18
5.2 PXRD measurement of indium sample from synthesis in Section 4.4 in **blue**, this has been plotted with a diffraction pattern of H_6cpb without any constituents in **green**. 18
5.3 FTIR measurement using ATR of dysprosium sample with H_6cpb from synthesis in Section 4.2. 20
5.4 FTIR measurement using ATR of yttrium sample with H_6cpb from synthesis in Section 4.2. 20
5.5 FTIR measurement using ATR of lanthanum sample with H_6cpb from synthesis in Section 4.2. 21
5.6 FTIR measurement using ATR of europium sample with H_6cpb from synthesis in Section 4.2. 21
5.7 FTIR measurement using ATR of lanthanum sample with H_6cpb from synthesis in Section 4.5. 22
5.8 TGA data on dysprosium sample from synthesis in Section 4.2. 23
5.9 PXRD measurement of indium sample from synthesis in Section 4.5 in **blue**, this has been plotted with a simulated powder diffraction pattern of MOF-894 using Mercury in **orange.** 23
5.10 PXRD measurement of magnesium sample from synthesis in Section 4.1 in **blue**, this has been plotted with a simulated powder diffraction pattern of MOF-889 using Mercury in **orange** 24
5.11 PXRD measurement of magnesium sample from synthesis in Section 4.2 in **blue**, this has been plotted with a simulated powder diffraction pattern of MOF-889 using Mercury in **orange** 24
5.12 PXRD measurement of H_6cpb without any other constituents in **green** and simulated powder diffraction patterns of crystallized H_6cpb with dmf in **blue** and with H_6cpb with dmf and acetate in **yellow**. 25

5.13 PXRD through SAXS measurement of dysprosium sample from synthesis in Section 4.2 in **blue**, this has been plotted with a diffraction pattern of H_6cpb without any constituents in **green**. 26
5.14 PXRD measurement of yttrium sample from synthesis in Section 4.2 in **blue**, this has been plotted with a diffraction pattern of H_6cpb without any constituents in **green**. 26
5.15 PXRD measurement of europium sample from synthesis in Section 4.2 in **blue**, this has been plotted with a diffraction pattern of H_6cpb without any constituents in **green**. 27
5.16 PXRD through SAXS measurement of lanthanum sample from synthesis in Section 4.2 in **blue**, this has been plotted with a diffraction pattern of H_6cpb without any constituents in **green**. 27
5.17 PXRD through SAXS measurement of lanthanum sample from synthesis in Section 4.5 in **blue**, this has been plotted with a diffraction pattern of H_6cpb without any constituents in **green**. 28
5.18 A fluorescent red light emitted by the europium sample from synthesis in Section. 4.2 when shining a 254 nm UV-light on the europium sample. . . 28
5.19 A fluorescent red light emitted by the europium sample from synthesis in Section. 4.2 shining a 302 nm UV-light on the europium sample. 28
5.20 A preliminary structure of CTH-17 without the counterions. Where **green** is lanthanum, **red** is oxygen and **grey** is carbon. 29
5.21 A preliminary structure of CTH-17 which illustrates the metal nodes as "rods". Where **green** is lanthanum, **red** is oxygen and **grey** is carbon. . . 30
5.22 The SBU of the metal nodes in CTH-17, Where **green** is lanthanum, **red** is oxygen and **grey** is carbon. 30

List of Tables

4.1 Synthesis data for the first synthesis using H_6cpb linker, at 120 °C with acetic acid and dmf as a media 13
4.2 Synthesis data for the second synthesis using H_6cpb linker, at 150 °C with acetic acid and dmf as a media 14
4.3 The stock solution of 0.5M of metal salts in water combined with H_6cpb linker used for synthesis. The mass of metal salt was calculated from the molar concentration of the stock solution 14
4.4 Synthesis data for the combinatory synthesis using H_6cpb and ppb linker, at 150 °C with acetic acid and dmf as a media 15
4.5 Synthesis data synthesis using H_6cpb linker, at 150 °C with acetic acid and dmf as a media 15

5.1 Sample results from synthesis, Only the samples which yielded precipitate is included in the table. Through analysis in SAXS it could be deduced that the samples were crystalline 16
5.2 Sample results from synthesis, by analyzing the samples in SAXS it could be deduced that the samples were crystalline. IR and TGA was done on the samples with yielded enough crystals to perform the analysis. 17
5.3 Sample results from synthesis, by analyzing the samples in SAXS it could be deduced that the samples were crystalline. IR and TGA was done on the samples with yielded enough crystals to perform the analysis 19
5.4 Calculated weight and mole for the sample containing dysprosium and H_6cpb from synthesis in Section 4.2 22

List of Abbreviations

kgd Kagome Dual.

ATR Attenuated Total Reflectance.

COFs Covalent-Organic Frameworks.

dcm dichloromethane.
dma dimethylacetamide.
dmf *N*,*N*-dimethylformamide.

FTIR Fourier Transform Infrared Spectroscopy.

GHGs Green House Gases.

H_6cpb 1',2',3',4',5',6'-hexakis(4-carboxyphenyl)benzene.

MOFs Metal-Organic Frameworks.

NIR Near Infrared.

ppb 4,4'-(3',4',5',6'-tetrakis(4-(pyridin-4-yl)phenyl)-4,4"-diyl)dipyridine.
PXRD Powder X-ray Diffraction.

SAXS Small Angle X-ray Scattering.
SBUs Secondary Building Units.
SCXRD Single-Crystal X-ray Diffraction.
SEM Scanning Electron Microscope.

TEM Transmission Electron Microscope.
TGA Thermogravimetric Analysis.

UV Ultraviolet.

1
Introduction

Modern materials are breaching into a new era of tailoring as chemists aim to refine materials for a specific purpose to raise the capabilities of current technologies. A strategy for development of such technologies is in reticular chemistry. Reticular chemistry is building a net-type structure where strong bonded discrete building units (such as molecules and clusters) are connected to make extended crystalline structures.[1] These systems include Covalent-Organic Frameworks (COFs), zeolites and MOFs. The focus in this project will be on MOFs.[2]

MOFs are often porous crystalline materials that are constructed from metal clusters (termed as Secondary Building Units (SBUs)) bonded by multidentate organic ligands. The combination SBUs and organic linker can form large, rigid and highly ordered net-type structures. These net-type structures exhibit physical properties of importance for tailoring materials and can be functionalized by introducing guest molecules to target specific functions of the structure.[3] In this project the synthesis of MOFs is based on a self-assembly approach by choosing appropriate metal ions and organic linkers in solvothermal synthesis. The capabilities and structural variety in MOFs come from the many combinations of SBUs and organic ligands that can be used. The vast range of combinations in synthesis allows for adaptation of the properties such as porosity and surface area which allows for target specific design.[4] This would allow MOFs to be a possible solution for modern problems such as more efficient solar panels or CO_2 adsorption.[5]

MOFs can be divided into the different basic geometrical topologies that their net structures are formed from, for example linear, triangle, square, hexagon. The simpler geometrical topologies have many reported structures of MOFs, while topologies such as the hexagon-based are less common. The reason for some topologies being scarcely reported is usually because of the lack of commercially available organic linkers which can form these topologies. The future of MOFs relies on exploring the possibility of creating different topologies to investigate properties and future applications. This thesis will focus primarily on the possibility of synthesizing reported and new hexagon-based topologies.[1]

1.1 Aim

Synthesis and development of MOFs based on selected metal ions and organic linkers to produce targeted metal-organic frameworks and investigate their properties. The focal point of the investigation is to form hexagon-based MOFs. The aim is then to determine the morphology and structural properties of any formed metal-organic frameworks. This would also include to analyze the obtained MOFs for potential use as in photo voltaic cells, CO_2-adsorption and I_2-adsorption. However, due to circumstances with COVID-19

pandemic the latter has not been a possibility.

1.2 Limitations

The project is limited to small scale synthesis of MOFs. The project will not go in to test the viability in any other applications, nor will there be any investigation of large-scale synthesis of MOFs. The project will investigate testing a solvothermal synthesis to form previously created MOFs with the intended linkers and investigate if other metals can be used and to optimize the synthesis.

The synthesis of organic molecules used as organic linkers will not be included in the project and the synthesis of the organic linkers will be made by Mr. Steffen Brülls.

The X-ray diffraction using Small Angle X-ray Scattering is in collaboration with Dr. Michal Starch at Chalmers Materials Analysis Laboratory.

1.3 Specification of issue under investigation

MOFs are generally produced using d-block metal ions. Other metals have been used to produce MOFs but the research is not as extensive and there is still much to be uncovered. This project will examine the possibility to produce the hexagon-based structure for more uncommon metals with a $+2$ or $+3$ oxidation state together with the intended linkers. Any new crystal structures with the intended linker may have unique properties. The metal groups in this project will include alkaline earth metals, lanthanoids, transition metals and d-block metals. More metals may also be incorporated in production as crystals might not be possible to form with mentioned metals and the intended linkers, attempts may then go back to the more common transition metals such as Cu.

2
Theory

This section will discuss relevant theory for MOFs and the analytical methods which are commonly used. It also includes potential applications for MOFs.

2.1 Reticular chemistry

The name reticular can be defined as "characterized by a fine network or netlike structure". Reticular chemistry is the study of net-type structures such as zeolites, COFs and MOFs. These net-type structures are made through linking molecular building blocks to make a crystalline open framework. The building blocks in these frameworks are termed as nodes which are polynuclear clusters which are connected with a linking molecule. The orientation of these nodes connected by an organic linker is termed SBUs.[1]

The SBU is the way that the metals are coordinated to each other and the organic linker. This provides rigidity and directionality to the structure and space arrangement of the MOF. SBUs are ordered in such a way that it also locks the geometry around the metal ions allowing a method of producing tailored MOF-structures. For example, a shape that produces large voids for gas adsorption could be tailored. Because the SBUs are formed by metal-carboxylate bonds the resulting structures are more thermally stable. This property combined with selectivity of the metals and linkers used allows for targeted structural functions. Optimization of any MOF synthesis involve the change of concentration, solvent polarity, pH and temperature.[6]

The many framework compositions of the building units introduce a design of the network topology. The design of these frameworks suffers from geometrical and connective constraints of the SBU to synthesize target MOFs. This requires appropriate combination of metal clusters and organic linkers and must account for the constraints for these compounds. The success rate for producing the topologies heavily relies on mapping compounds suitable for producing frameworks and the availability of organic and inorganic building units.[7]

2.2 Metals

2.2.1 Alkaline earth metals

The coordination chemistry of alkaline earth metals still remains largely unexplored and as for Mg-based MOFs only a few structures have been reported.[8] Magnesium has a +2 oxidation state and because of its reactivity with acids it is possible for Mg to produce SBUs by reacting with the carboxylate group in the linkers. Previously Mg-MOFs have

shown to rival competitive materials of CO_2 capture, with high selectivity and among the highest dynamic capacities of porous materials.[9] A magnesium-based MOF with H_6cpb as a linker has already been synthesized and is called MOF-889.[10]

2.2.2 Chromium

Chromium-based MOFs are of interest for the robustness, porosity and redox properties. However only a few Cr-based MOFs have ever been produced because of difficulties in synthesis owing to the kinetic inertness of the Cr-O bond. The chromium oxides is also the most commonly used for industrial purposes and the lack of other application for Cr-MOFs has also been a contributing factor to the absence of research for this metal.[11] Previous methods of synthesizing Cr-MOFs have been done in an oxygen free environment to prevent any Cr-O from forming.[12]

2.2.3 Lanthanoids

Lanthanoids have been studied for the interesting properties that comes from the 4f electrons which give lanthanoids unique characteristics such as fluorescence and strong magnetic properties. In today's society lanthanoids are essential components for numerous technological devices and is used in everything from wind turbines to cellphones.[13] Lanthanoid-organic frameworks have previously shown unique luminescence properties. Due to their sharp emission, large stokes shift and high color purity from the 4f electron shell these MOFs could be considered as effective luminescent probes for technological devices. One of the primary metals for this research is europium for the characteristic emission within the visible spectra from Ultraviolet (UV) to Near Infrared (NIR).[14,15]

2.2.4 Yttrium

Yttrium is a d-block metal however, it is also considered as a rare earth metal with properties and coordination chemistry more like that of lanthanoids especially in the +3 oxidation state. Yttrium similarly to lanthanoids is also an element commonly used in technological devices. Previously reported work on Y-MOFs has doped the MOFs with lanthanoids such as Tb or Eu for tunable photoluminescence[16]

2.2.5 Indium

Indium-organic frameworks have been previously studied for their adsorption capabilities but also for fluorescence, ion-exchange properties and Lewis acid catalysis. In-MOFs show high surface area and high chemical stability which makes them interesting for MOF development. Previously produced MOF with In and the linker H_6cpb has been produced and is called MOF-894. In adsorption testing of this MOF it proved to have a low surface area due to the counter ions required to form the MOF.[17,18]

2.3 Linkers

The organic linkers used will be centered around the organic linker H_6cpb seen to the left in Figure 2.1. The linker is conformationally chiral and has been previously proven to produce **htp** and **hhp** nets which has previously proved to have a high CO_2-selectivity.[7,10]

Similar organic linker to H_6cpb is 4,4'-(3',4',5',6'-tetrakis(4-(pyridin-4-yl)phenyl)-4,4"-diyl)dipyridine (ppb) seen to the right in Figure 2.1. The ppb linker is a conformationally chiral molecule and is missing carboxylate groups which prevents the formation of MOFs with only this linker and it will be used in combination with H_6cpb. The linkers are flat hexagon shaped building blocks which may produce hexagon topology. The H_6cpb linker have shown previously to produce the Kagome Dual (**kgd**) net and other similar nets which have already been documented. However, the structures are still of great interest because of the remarkable capabilities and void spaces that has been formed using the **kgd**, **hhp**, **yav** and **htp** topology. There may also still be new variations to already existing networks.[18,10]

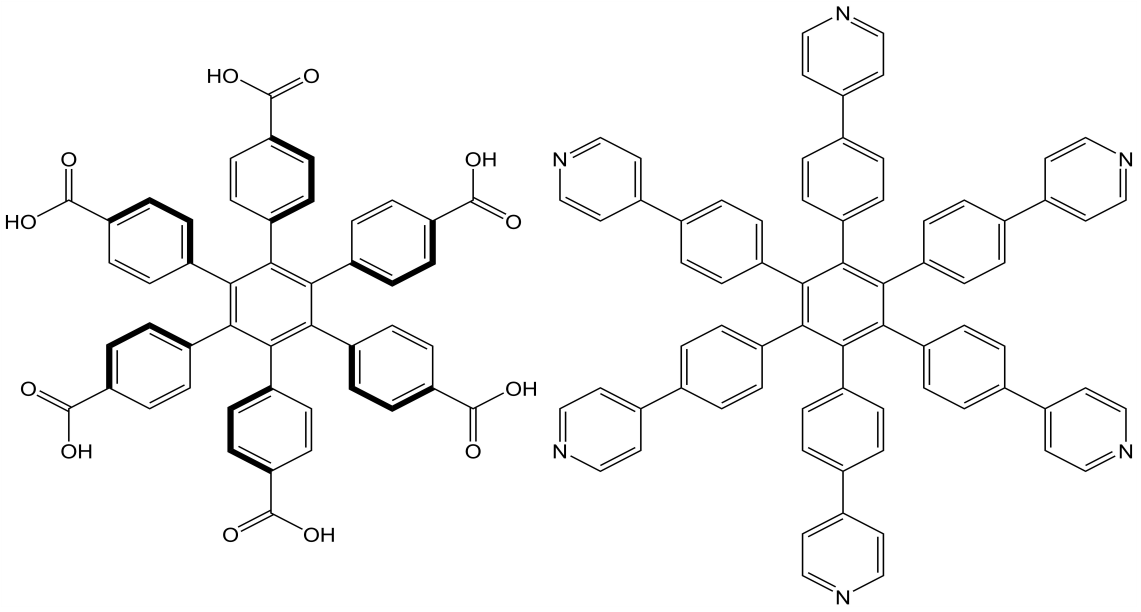


Figure 2.1: The hexatopic organic linker 1',2',3',4',5',6'-hexakis(4-carboxyphenyl)benzene called H_6cpb to the **left**. The organic linker 4,4'-(3',4',5',6'-tetrakis(4-(pyridin-4-yl)phenyl)-4,4"-diyl)dipyridine called ppb to the **right.**

2.4 Characteristics

The investigations regarding MOFs will focus on producing hexagon-based topologies. The interest in hexagon shapes originates from the fact that they are uncommon in comparison to other basic shapes.[1] The intended linkers will verify if there is a characteristic molecular structure needed to produce hexagon topologies, that is a hexagonal building unit. A specific topology found in hexagon structure is the **kgd** topology. The **kgd** net consists of two nodes: a trigonal (3-c) and an hexagonal (6-c).[7] By using these nodes **kgd** net can be formed as in Figure 2.2.

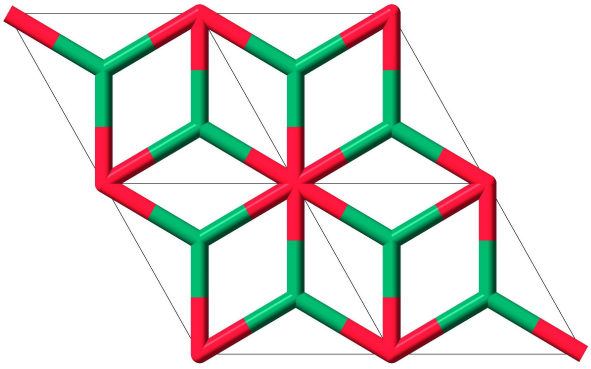


Figure 2.2: Trigonal (3-c) in **green** and hexagonal (6-c) in **red** are the building units to build the **kgd** net.

A MOF which produces a **kgd** network which is relevant to this project would be the indium based MOF denoted MOF-894.[18] The 3-D network of this MOF is based on stacking the **kgd** layers. Like the 3-D **kgd** MOFs, while not stacking the **kgd** layers would be a net called **laf** of the space group $P4_2/m\ n\ m$ which is of interest. The reason for this is that the **laf** net can be folded without breaking any bonds, however when folded the projection would form a **kgd** network with the same angles and building units. This is because the **laf** net is composed of perfect hexagons combined with perfect equilateral triangles. This means the configuration in 3-D would consist of unit cell lattices being perpendicular to each other this can be seen in Figure 2.3. This would give it the possibility to fold from a 3-D structure into a 2-D **kgd** net. This type of flexibility could give a crystal the ability to increase in volume as molecules adsorb. This would also give the possibility of a stable structure with immense voids between each of lattice plane. These structures of the 3-D unit cells have been drawn using CrystalMaker show the MOF topology.[19]

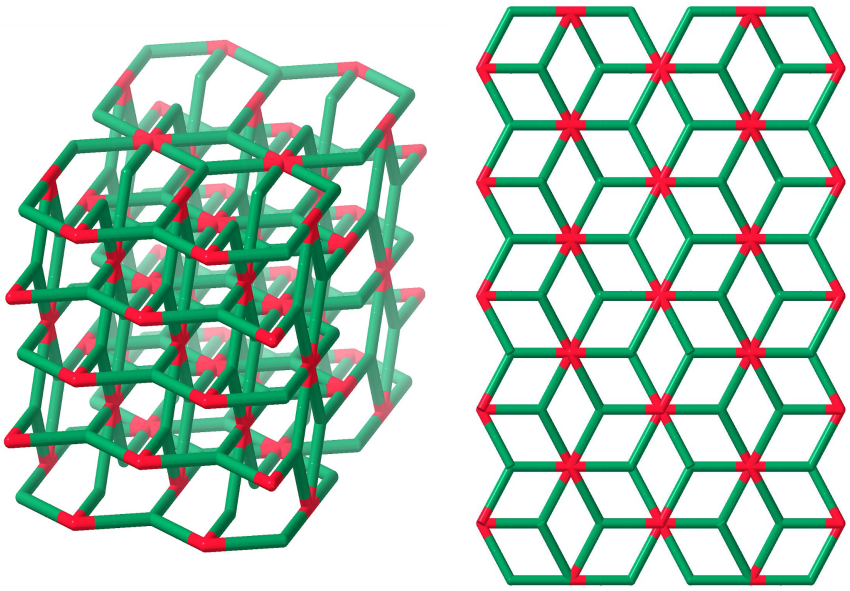


Figure 2.3: The **laf** net in the image to the **left**. The same configuration when folded to the **right**.

While there are several 3-D nets which have a similar 2-D appearance to the **kgd**, they differ in either the building units needed to build a **kgd** structure or the angles between

each of the building units[10]. The relevant one for this project would be the **yav** structure which is adopted by the magnesium-based MOF denoted MOF-889. As seen in Figure 2.4 This structure looks similar to a **kgd** and also build 3-D network through stacking of the layers. The nodes consists of a trigonal bipyramid (5-c) node and an hexagonal (6-c) node.[19]

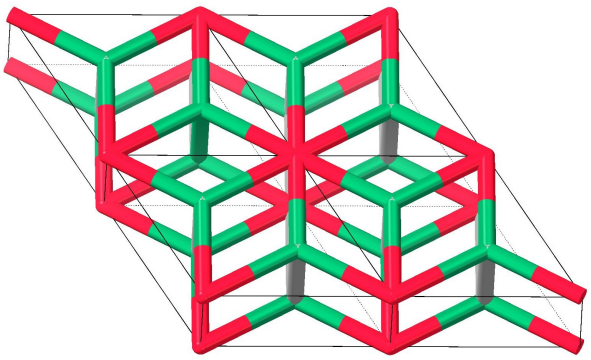


Figure 2.4: Trigonal bipyramid (5-c) in **green** and hexagonal (6-c) in **red** are the building units to build the **yav**.

2.5 Solvothermal synthesis

The method of synthesis for MOFs that will be used in this project is solvothermal synthesis. This is the most common method for synthesis of MOFs but also for other self-assembling systems. This method is good for self-assembling systems because these systems are far to large for a step by step synthesis. It is a simple approach of adding the metals and linkers into a solution and heating them over an extended period. In this time the metal complex ligands will dissociate in Lewis acid-base reaction and the carboxylate bond in the linkers will bind to the metal cation through the same reaction. The MOF is then formed through self-assembly where the new metal complexes and linkers will coordinate to a MOF from their random initial placement in the solution.[20]

2.6 Modes of analysis

This section will discuss the methods used for analysis of samples that are commonly used to analyze MOFs and crystals of other reticular compounds.

2.6.1 Crystal diffraction analysis

Single-Crystal X-ray Diffraction (SCXRD), PXRD and electron diffraction are the main analysis used to identify the formed MOFs but they are suitable for most crystalline samples.

All kinds of X-ray diffraction work by using a radiation source which provides the incident X-ray beam. The radiation source commonly found is a sealed tube from which electrons are emitted from a tungsten filament. The electrons are accelerated towards a metal target (anode) and when they strike the target the inner shell electrons are displaced and higher energy electrons from outer orbitals takes its place. When the electrons from out

orbitals enter a lower orbital, they also lower their orbital energy and produce x-ray photons. The most common metal targets are Cu and Mo, which emit characteristic X-rays ($\lambda = 1.54$ Å and $\lambda = 0.71$ Å respectively) which then can be filtered and concentrated into a monochromatic beam of X-rays that is focused on the target sample. The interaction between the incident X-ray beam and the sample reflects the X-rays by constructive interference which satisfies Bragg's law in Equation. 2.1 Diffracted X-rays are processed and counted as the sample is scanned and the relationship between the diffraction geometry and the crystal lattice can then be calculated.[21]

$$\lambda = 2d_{hkl}\sin(\theta_{hkl}) \tag{2.1}$$

SCXRD provides a three dimensional image of the crystal structure including unit cell dimensions, atomic coordinates and site-ordering.[21] Instead of only using one angle to measure the diffraction pattern is measured using four different angles (2θ, χ, ϕ, and Ω) through the use of a goniometer which can spin the sample. With the different angles an exact mapping of the angles can be made.[21]

Powder diffraction scans the θ-angle and gives a diffraction pattern unique to the crystal, however routinely the cell dimensions can be confirmed using this method. This means that only previously identified crystals which already has a set powder diffraction pattern can be solved using this method. Identification of a structure could be done using PXRD through the use of CrystalMaker or similar programs which can simulate a PXRD pattern however this may be difficult due to the many possible structure.[21]

Electron diffraction is especially useful when there are small crystals. An electron microscope such as a TEM or Scanning Electron Microscope (SEM) is used to scan the surface of the crystals. An elemental analysis and XRD can be done with this method on nanoscale samples.[21]

Small Angle X-ray Scattering (SAXS) is a machine used which measures the intensities of X-rays scattered by a sample similarly to a PXRD. A SAXS machine is used for small angle measurements between 0.1°-5°which is not commonly measured by a PXRD. This makes a SAXS machine ideal for measuring nanoscale densities and low energy conformations which form in crystal lattices. The main detector to beam line can be setup to measure angles between $0.1° \leq 2\theta \leq 30°$. However, the SAXS machine can be used to measure higher angles by using a secondary detector which is located above the sample instead of being aligned with the sample. The secondary detector makes it possible to measure from $28° \leq 2\theta \leq 85°$. This makes it possible to measure MOF signals at low 2θ-angles with excellent quality while still measuring the full range of a PXRD pattern.

2.6.2 Fourier Transform Infrared Spectroscopy

FTIR is a method of analysis which measure the interaction between electromagnetic radiation source and a sample. Interactions with the substance can provide information on the molecular structure and energy level transmission. The measurement is done using an infrared beam which is absorbed in the sample and will transmit light, this light will then register in the detector. Through Fourier transformation the data can be transformed into a spectrum which can be used to identify certain chemical structures present in a compound.[22]

2.6.3 Thermogravimetric analysis

TGA is a thermal method of analysis which is used to provide information about physical and chemical properties. TGA measures the mass of a sample over time while the temperature changes. This method is mainly used to determine the stability of the MOF by detecting the thermal decomposition. But it can also be used for absorption, adsorption and desorption measurements.[23]

2.7 Potential applications

2.7.1 I_2-sorption

Uranium fission in nuclear reactors is one of the primary sources for energy. Large amounts of radioactive isotopes of iodine (mainly ^{131}I) are generated as a by-product of uranium fission.[24] From nuclear accidents and radioactive waste, radioactive isotopes of iodine is released into the atmosphere. The release of iodine may then affect humans through inhalation and 10-30% of iodine intake accumulate in the thyroid gland. The accumulated iodine will continue to decay which may cause harm to the thyroid and surrounding tissue.[25] To prevent this there is a need for new adsorption methods of iodine. MOFs show great potential as solid porous material with tunable properties, it may provide a solution to this issue.[26]

2.7.2 CO_2-sorption

The growing population and industrialized society have led to an trend of increasing CO_2 and other Green House Gases (GHGs) emissions. The greenhouse effect caused by the emissions threaten the world with a climate change and an increase of the temperature globally. The increase of temperature will indirectly free CO_2 trapped in arctic permafrost on top of this the industry is ever increasing the release of GHGs. Trees have a natural way of dealing with the CO_2 but with an increase in deforestation and CO_2 emissions, the concentration of CO_2 will continue to increase. Different approaches have been discussed to tackle this issue. One of them being to capture the CO_2 with the help of adsorbing materials for underground storage. This may be possible with solid adsorption of CO_2 gas in MOFs, COFs and zeolites.[27]

2.7.3 Solar Cells

Today there is a concern for the growing energy shortage and producing sustainable energy in an environmentally conscious way. Solar cells and photo voltaic devices work by converting optical signals into electric currents. The most common photo voltaic devices are currently composed out of silicon material that absorbs a spectrum of wavelength emitted by the sun.[28] MOFs have been introduced into these systems mainly as photo active material. They have been introduced to increase the absorbance in the region from visible light to NIR and therefore improve the efficiency of photo voltaic devices. The primary research on MOFs for solar cell application is focused on lowering the band gap energy for the crystals and to increase the chemical stability. Incorporation of guest molecules such as large dyes and catalytically active coordination compounds have also been introduced to enhance proton conductivity within MOFs.[29]

3
Methodology

3.1 Synthesis of MOFs

The synthesis was done through the solvothermal reaction. The synthesis methodology was previously developed at this department by Dr. Francoise Noa.

The solvent used for the synthesis is *N*,*N*-dimethylformamide (dmf) and acetic acid. dmf is primarily used because it is a polar aprotic solvent which allows for both metal salt and linker to be dissolved without there being any hydrogen ions in solution. Acetic acid is primarily used because it is acidic enough for the Lewis acid-base reaction to occur but weak enough not to interfere with the carboxylic acid in the linkers bonding to form a metal complex.

Before the synthesis starts the metal salt and linker is weighed and the constituents keep to a molar ratio. Different ratios have been used throughout the project, this was done to see if larger crystals would form and to decrease the likelihood of unreacted linker in the samples. The linker was added to a glass vial of dmf which was heated to 100 °C and stirred until the mixture was clear. The weighed metal salt and additional dmf was added. The amount of dmf in the solution is dependent on how dilute the solution should be. A more dilute solution usually takes a longer time to form crystals. After this acetic acid and dmf was added to the solution in a 1:1 volume ratio. It is used to keep the solution acidic and to neutralize any counter ions from the metal salt. The glass vial was heated and stirred until a clear mixture had formed. The solution was then transferred into a autoclave or microwave reaction vial with a crimp cap. The reaction vessel was then placed in an oven at 120-150 °C for a period of 1-31 days. The temperature and time the sample was in the oven was paramount for the reaction. Even at a higher temperature the reaction may still require a long time in the oven because of the slow formation rate of some MOFs.

3.2 Filtration

To ensure that all the solvent was removed, several triturations were done in dichloromethane (dcm). The solution was poured through a filter paper where the runoff goes into a beaker. The crystals were then washed several times with dcm until all the dmf has been removed. After drying the filter paper in the fume hood, the crystals were transferred from the filter paper into a small vial containing dcm. Samples which were produced using a chloride salt were triturated with methanol according to the same procedure. This was done due to crystals dissolving in dcm.

3.3 Drying

To perform any of the methods for analysis the crystals would need to be dried. This was done through taking out some of the sample with a pipette. The sample was then put on a microscope glass plate where it was left to dry in the fume hood. After drying, the powder residue left on the microscope glass plate was scraped together and then tested.

3.4 Methods for characterization

The plan for characterization was to use SCXRD to determine lattice parameters and crystal structure of the samples. Following this a PXRD would then be done to determine crystal homogeneity and further evaluation. Other analysis that would be carried out following this would be elemental analysis, I_2-sorption and CO_2-sorption. However due to the circumstances of the COVID-19 the possibility of running SCXRD and elemental analysis has been eliminated.

3.5 Thermogravimetric analysis

The TGA was done to assess the thermal stability of the MOF. The TGA were performed in Mettler Toledo TGA/DSC 3+. The MOF was heated from 30°C to 800°C using a air flow of 60 ml/min with a temperature increase of 10 °C/minute. Because of the high temperature used in the TGA an alumina crucible was used

3.6 Fourier Transform Infrared Spectroscopy

The FTIR was performed with dry powder using Attenuated Total Reflectance (ATR). In measurements the infrared beam passes through the sample and into the ATR crystal. The light passes through the ATR crystal which reflects the light inside the crystal and then hits the detector as infrared light. ATR operates through measuring the changes of the internally reflected beam when the ATR is in contact with the sample. ATR was used due to the simplicity and fast analysis of the sample. Dried sample was used to perform the measurements on a Thermofisher FTIR. Absorbance of IR light between 400 cm^{-1}-4000 cm^{-1} was measured.

3.7 PXRD through SAXS

In order to assess the structure of the obtained compounds, X-ray diffraction experiments were carried out. MOF signal is expected at very low 2Θ-angles due to the structural properties of the studied compounds, this is due to the large network formed by MOF which results in a high lattice constant. PXRD patterns in transmission were acquired using the SAXSLAB Mat:Nordic instrument equipped with a micro-focus Cu X-ray source (λ=1.54Å) and a Dectris Pilatus 300K R (3°$\leq$ 2Θ $\leq$30°- in line with the beam) and 100K R (28°$\leq$ 2Θ $\leq$85°- mounted on a motorized goniometer) detectors. The entire beam path was evacuated before each measurement to 0.2 mbar to minimize air scattering, which allowed for excellent data quality even at very low angles. The sample position was

calibrated before each measurement series using silver behenate and alpha-Al_2O_3 powders. For each MOF sample, the exposition time was 20 min for both the 300K R detector, and the 100K R detector. These were placed first at an angle of 39°and next at 57°from the beam, covering an angular 2Θ range of 28°-50°and 46°-68°respectively. The obtained 2D images where integrated using standard approaches with the Saxsgui software, and the resulting patterns were merged together. While averaging the overlapping sections and adjusting the intensities based on alpha-Al_2O_3 reference pattern. This method was used throughout the project instead of using a regular PXRD because of the small sample sizes used.

3.7.1 Capillaries

The first method tried for SAXS was using capillaries where the dried crystalline samples were loaded in the capillaries. The capillaries were then taped to the standard SAXS sample plate for measurement. This methodology was not kept because of the trouble loading the capillaries with the sample. It proved to be difficult to have enough sample gather at a single spot in the capillaries to carry out measurements.

3.7.2 Transparent adhesive tape method

Transparent adhesive tape was used to collect the crystals from the glass slide. Another tape was placed on the tape to form 2 layers and to keep the sample in place. This was then taped to a standard SAXS sample plate. For reference 2 layers was used as a reference and subtracted post-treatment.

4
Experimental

Different methodologies have been tried in this thesis in order to produce MOF crystals of adequate size with the intended linker and metal salts. The different methodologies have been taken from previous reports of MOF production however the recipe may be modified. Analysis of the samples was done with analytical methods stated in Section 2.6. The different synthesis and analysis approaches will be discussed in this chapter and the results can be seen in Chapter 5.

4.1 Synthesis with hexatopic H_6cpb

The H_6cpb and metal salts are included in a solvothermal reaction in a solution of dmf with acetic acid as a media. The metal and linkers were dissolved in a 2:1 ratio with 1 ml of dmf. The solutions were stirred at 120 °C until it was clear and homogeneous. An additional 1 ml of dmf and acetic acid was added. The mixtures were again stirred to assure a homogeneous solution. The solutions were then sealed in microwave reaction vials using a crimp-top cap and were heated in the oven for the formation of the MOF through self-assembly. The heating was put to 120 °C and the samples were left in the oven until a precipitate had formed. The different metals attempted with this synthesis can be seen in table 4.1.

Table 4.1: Synthesis data for the first synthesis using H_6cpb linker, at 120 °C with acetic acid and dmf as a media

Metal salts	**Chemical formula**	**Metal salt** [mg]	**H_6cpb** [mg]	**Reaction Time** [d]	**Precipitate**
Chromium(III) chloride	$CrCl_3$	6.3	16.0	18.0	No
Chromium (III) nitrate hydrate	$Cr(NO_3)_3 \cdot 9H_2O$	16.0	16.1	>30	No
Europium(III) nitrate hydrate	$Eu(NO_3)_3 \cdot 5H_2O$	17.3	16.0	18.0	Yes
Indium(III) chloride	$InCl_3$	8.8	16.2	>30	No
Magnesium (II) acetate hydrate	$(CH_3COO)_2Mg \cdot 4H_2O$	8.8	16.1	18.0	Yes
Magnesium (II) nitrate hydrate	$Mg(NO_3)_2 \cdot 6H_2O$	6.3	16.0	18.0	Yes
Lanthanum (III) nitrate hydrate	$La(NO_3)_3 \cdot 6H_2O$	17.4	16.0	18.0	Yes

4.2 High temperature synthesis with hexatopic H_6cpb

The second synthesis using H_6cpb and metal salt, the reaction conditions were changed. The metal and linkers were dissolved in a 3:1 ratio with 0.5 ml of dmf. The solution was stirred at about 100 °C until it was clear and homogeneous. An additional 0.5 ml of dmf and 1 ml of acetic acid was added. For indium chloride and chromium chloride 1 ml formic acid was used instead of acidic acid. This was done to force the Lewis acid-base reaction by using a stronger acid due to previous samples not yield any precipitate. The mixtures were stirred again to assure a homogeneous solution. The solutions were then sealed in microwave reaction vials using a crimp-top cap and were heated in the oven to for the formation of the MOF through self-assembly. The heating was put to 140 °C

and the samples were left in the oven until a precipitate had been formed. The different metals attempted with this synthesis can be seen in Table 4.2.

For the europium and the lanthanum samples of this synthesis, the samples were run in available autoclaves using a heating program in Memmert UN75plus oven. The heating program increased the temperature with a gradient from 20 °C to 120 °C over 2 hours. The sample was then heated for 168 hours at 150 °C. The cooling was also done with a gradient from 150 °C to 20 °C over 20 hours.

Table 4.2: Synthesis data for the second synthesis using H_6cpb linker, at 150 °C with acetic acid and dmf as a media

Metal salts	**Chemical formula**	**Metal salt** [mg]	**H_6cpb** [mg]	**Reaction Time** [d]	**Precipitate**
Chromium (III) nitrate hydrate	$Cr(NO_3)_3 \cdot 9H_2O$	12.0	7.9	8.0	No
Dysprosium (III) nitrate hydrate	$Dy(NO_3)_3 \cdot xH_2O$	10.5	8.1	8.0	Yes
Europium (III) nitrate hydrate	$Eu(NO_3)_3 \cdot 5H_2O$	12.9	8.1	8.0	Yes
Indium (III) chloride	$InCl_3$	6.7	7.9	>8	No
Lanthanum (III) nitrate hydrate	$La(NO_3)_3 \cdot 6H_2O$	13.0	8.2	8.0	Yes
Magnesium (II) nitrate hydrate	$Mg(NO_3)_2 \cdot 6H_2O$	7.7	7.9	8.0	Yes
Yttrium (III) nitrate hydrate	$Y(NO_3)_3 \cdot 6H_2O$	11.5	8.0	8.0	Yes

4.3 Synthesis of MOF-889

The synthesis of MOF-889 follows a synthesis route similar to that in the article by P. Nguyen et al.[10] A stock solution of 0.5 M solution of magnesium (II) nitrate hydrate in deionized water (0.12 mL) was added to a 10 mL vial which contains the organic linker H_6cpb (8 mg, 0.01 mmol). The following is added to the vial: dmf (0.40 mL), MeOH (1.50 mL) and deionized water (0.12 mL). The solution is mixed with a stir bar at 100 °C until the mixture is clear. The mixture is then transferred to a microwave reaction vial more suitable for heating and sealed with a crimp top cap. The solution was then left in the oven at 120 °C for 7 days. The same procedure and concentrations were tried with chromium (III) nitrate hydrate.

Table 4.3: The stock solution of 0.5M of metal salts in water combined with H_6cpb linker used for synthesis. The mass of metal salt was calculated from the molar concentration of the stock solution

Metal salts	**Chemical formula**	**Metal salt** [mg]	**H_6cpb** [mg]	**Reaction Time** [d]	**Precipitate**
Chromium (III) nitrate hydrate	$Cr(NO_3)_3 \cdot 9H_2O$	24.0	8.1	1.0	Yes
Magnesium (II) nitrate hydrate	$Mg(NO_3)_2 \cdot 6H_2O$	15.4	8.1	7.0	Yes

4.4 Synthesis using H_6cpb & ppb

An attempt of mixing linkers was suggested from previous testing at the department. A mixture of the linkers H_6cpb and ppb with different transition metals was used to increase the likelihood of producing a MOF. The metals used were nickel, iron, copper and manganese. The direct synthesis approach was used in this synthesis and the molar ratio was 1:1.25:2 of H_6cpb:ppb:Metal salt. The metal salts used in combination with the linkers can be seen in Table 4.4 where several of the samples showed crystalline precipitates after the reaction time. However, it was discovered during filtration that the crystals were very small. This proved an issue because the crystals would sink into the pores of the filter paper without any possibility for extraction. The filtration was first attempted with a sample which had hardly any precipitate that was believed to be the reason for this occurrence. Another sample with a substantial amount of precipitate was also tested with

the same results. This resulted in a loss of two samples and the remaining samples were not filtered. A solvent exchange was performed through centrifugation to form a cake at the bottom of the test vial. As much supernatant as possible was removed with a pipette without removing any of the crystalline sample. The vial was then filled with methanol for faster drying procedure and testing in PXRD.

Table 4.4: Synthesis data for the combinatory synthesis using H_6cpb and ppb linker, at 150 °C with acetic acid and dmf as a media

Metal salts	**Chemical formula**	**Metal salt** [mg]	**H_6ppb** [mg]	**H_6cpb** [mg]	**Reaction Time** [d]	**Precipitate**
Chromium (III) nitrate hydrate	$Cr(NO_3)_3 \cdot 9H_2O$	3.2	5.1	3.4	23.0	Yes
Nickel (II) nitrate hydrate	$Ni(NO_3)_2 \cdot 9H_2O$	2.3	5.1	3.2	27.0	Yes
Iron (III) nitrate hydrate	$Fe(NO_3)_2 \cdot 9H_2O$	3.2	4.9	3.1	23.0	Yes
Manganese (II) chloride	$MnCl_2 \cdot 4H_2O$	1.6	5.2	3.1	27.0	Yes

4.5 Synthesis of lanthanum and indium with H_6cpb

This synthesis was made using the method in Section 4.2 but the ratio of metal to H_6cpb was changed from 3:1 to 4:1.

Previous attempts of synthesis with indium and H_6cpb yielded no crystals in the microwave vials. A synthesis was done in an autoclave to see if this would produce crystals.

Synthesis with lanthanum and H_6cpb had previously yielded crystals but a low quantity. Because of this there was only enough sample to do a PXRD and FTIR analysis. The PXRD of this sample had resulted in interesting peaks seen in Section 5.8, Figure 5.16. Because of this, a larger synthesis in autoclave was done where the volumes where increased by a factor of 5 and the amount of solvent was increased from 1 ml of both acetic acid and dmf, to 6 ml of each of the solvents. This was done to produce a larger quantity of crystals for further testing.
The experimental data from each synthesis can be seen in Table 4.5.

Table 4.5: Synthesis data synthesis using H_6cpb linker, at 150 °C with acetic acid and dmf as a media

Metal salts	**Chemical formula**	**Metal salt** [mg]	**H_6cpb** [mg]	**Reaction Time** [d]	**Precipitate**
Indium (III) chloride	$InCl_3$	8.9	7.9	14	Yes
Lanthanum (III) nitrate hydrate	$La(NO_3)_3 \cdot 6H_2O$	30.0	65.1	11	Yes

5
Results and Discussion

In this chapter the results presented will be from the synthesis and analysis of the samples. Comparison with references from other reports will also be made in this section.

5.1 Synthesis with hexatopic H_6cpb

In this synthesis magnesium produced white crystalline precipitate after heating, while the lanthanum and europium yielded small white crystalline precipitate. Images of these can be found in Appendix 1. This synthesis yielded crystals in accordance with Table 5.1. Due to evaporation of solvent, both the lanthanum and europium precipitate was lost before being able to measure the sample. When preparing the capillaries of the remaining samples, the samples of magnesium acetate was lost due to breaking one of the capillary. This resulted in measuring only one of the samples from the first synthesis. Due to difficulty setting up the machine to measure capillaries, the result from the first measurement was only being able to tell if the sample was crystalline. However, at the end of the thesis this sample was remeasured through mounting the capillary differently. The results can be found in Section 5.8.

Table 5.1: Sample results from synthesis, Only the samples which yielded precipitate is included in the table. Through analysis in SAXS it could be deduced that the samples were crystalline

Metal salts	**Chemical formula**	**Observations**	**Crystalline**
Europium (III) nitrate hydrate	$Eu(NO_3)_3{\cdot}5H_2O$	Small white precipitate	-
Magnesium (II) acetate hydrate	$(CH_3COO)_2Mg{\cdot}4H_2O$	White precipitate	-
Magnesium (II) nitrate hydrate	$Mg(NO_3)_2{\cdot}6H_2O$	White precipitate	Yes
Lanthanum (III) nitrate hydrate	$La(NO_3)_3{\cdot}6H_2O$	Small white precipitate	-

5.2 High temperature synthesis with hexatopic H_6CPB

This synthesis yielded crystalline samples in accordance with Table 5.2. The analysis made of the samples were based on the amount of precipitate which was produced. Because of the small sample size of the synthesis, IR and TGA could not be run on all the samples. Another synthesis would be required to test these samples again through TGA and IR, however it was not prioritized to do more synthesis because SCXRD was not available for the thesis. This means that it is pointless to perform IR and TGA analysis because these methods of analysis will not conclusively prove if the resulting crystals are MOFs.

Table 5.2: Sample results from synthesis, by analyzing the samples in SAXS it could be deduced that the samples were crystalline. IR and TGA was done on the samples with yielded enough crystals to perform the analysis.

Metal salts	**Chemical formula**	**Observations**	**Crystalline**	**IR**	**TGA**
Dysprosium (III) nitrate hydrate	$Dy(NO_3)_3{\cdot}xH_2O$	Small white precipitate	Yes	Yes	Yes
Europium (III) nitrate hydrate	$Eu(NO_3)_3{\cdot}5H_2O$	Small white precipitate	Yes	Yes	No
Lanthanum (III) nitrate hydrate	$La(NO_3)_3{\cdot}6H_2O$	Small white precipitate	Yes	Yes	No
Magnesium (II) nitrate hydrate	$Mg(NO_3)_2{\cdot}6H_2O$	white precipitate	Yes	No	No
Yttrium (III) nitrate hydrate	$Y(NO_3)_3{\cdot}6H_2O$	white precipitate	Yes	Yes	No

5.3 Result from synthesis of MOF-889

The procedure for MOF-889 produced small white crystalline powder which was expected as the procedure was similar to the from P. Nguyen et al.[10] In the end the crystals could not be tested because all the solvent evaporated and produced a brown powder where the precipitate were previously white. This is believed to be degraded product.

The chromium sample followed the same procedure as that of magnesium and produced a gel after one day. The gel was transferred into a drying vessel and was left to dry on a hotplate for one week. This left crystalline residues which were scraped off and suspended in DCM. The analysis of this chromium show that the crystalline residue was amorphous material. Image of these can be found in Appendix 1.

There was no continuation of this procedure because the H_6cpb has previously proved that for +3 charged metal ions a higher temperature is needed of about 150 °C. When using water and methanol as the primary solvents the risk of burning the samples because of the fast evaporation under these conditions were considered likely.

5.4 Results from synthesis using H_6cpb & ppb

The synthesis using a combination of H_6cpb and ppb resulted in microscopic black precipitate forming after the reaction time. There was a small quantity of precipitate which had formed after only a week. However, the samples were left in the oven further to ensure that all constituents had reacted. The small quantity of precipitate formed was enough to perform a PXRD measurement according to the method in Section 3.7.

In Figure 5.1 the PXRD measurement of the nickel sample can be seen. The sample exhibit no apparent crystal peaks, the microscopic precipitate may be a reason for the sample not showing any significant peaks. However, it is more likely that this sample is amorphous.

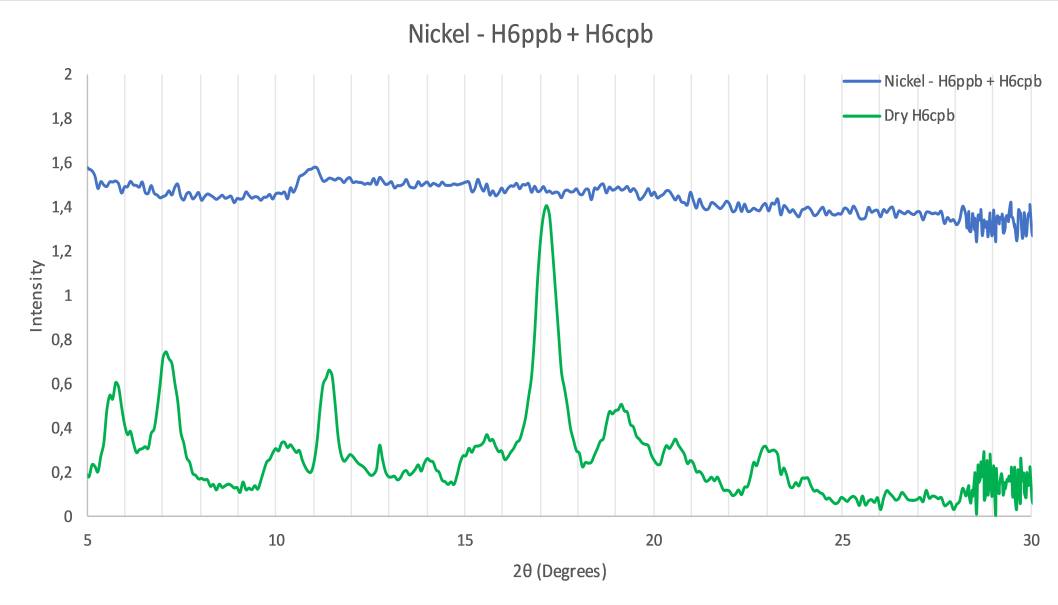


Figure 5.1: PXRD measurement of Nickel sample from synthesis in Section 4.4 in **blue**, this has been plotted with a diffraction pattern of H_6cpb without any constituents in **green**.

In Figure 5.2 the PXRD measurement of the manganese sample can be seen. This sample show apparent crystalline peaks which do not match to the dry H_6cpb measurement. The crystal product produced in this sample could be a MOF structure which only uses one of the linkers. H_6cpb with manganese have shown promising results to produce MOFs in the work by Victor Engdahl.[30] It is also entirely possible that the crystal structure has been produced using both linkers. This would show that a combination synthesis of these two linkers could lead to new MOF structures which have not previously been synthesized.

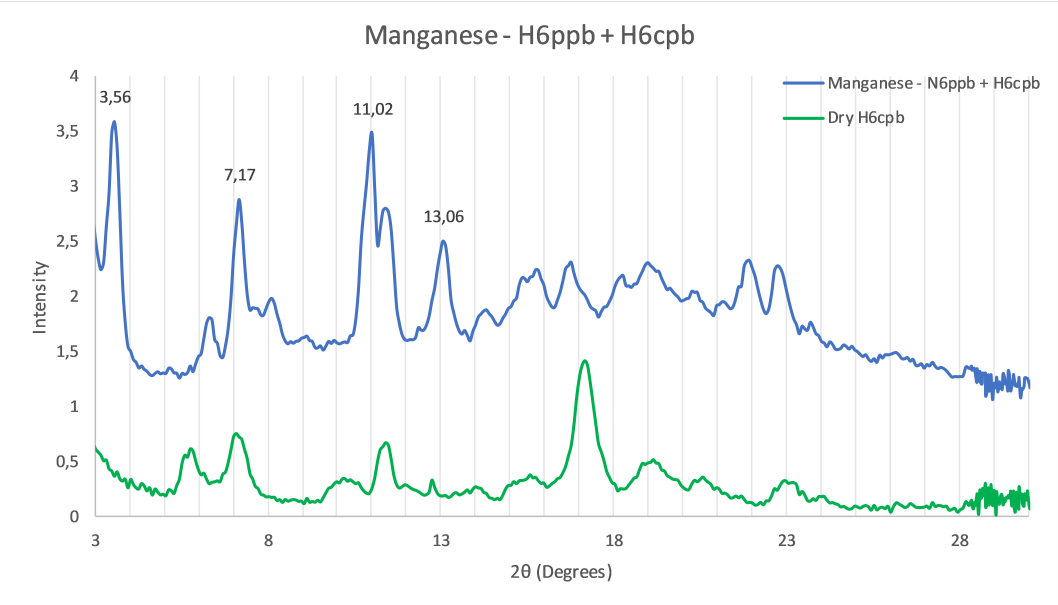


Figure 5.2: PXRD measurement of indium sample from synthesis in Section 4.4 in **blue**, this has been plotted with a diffraction pattern of H_6cpb without any constituents in **green**.

5.5 Results from synthesis of lanthanum and indium with H_6cpb

The results of synthesizing indium with H_6cpb in an autoclave resulted in crystalline precipitate. An image of these crystals can be found in Appendix 1. The PXRD measurement can be seen in Figure 5.9. Because of the small sample size TGA and IR could not be run on the sample.

The scaled-up synthesis of lanthanum with H_6cpb in autoclave resulted in a large quantity of crystalline precipitate. The PXRD measurement can be seen in Figure 5.17 and IR measurement in Figure 5.7. This sample was also tested through electron diffraction crystallography to determine a preliminary structure.

Table 5.3: Sample results from synthesis, by analyzing the samples in SAXS it could be deduced that the samples were crystalline. IR and TGA was done on the samples with yielded enough crystals to perform the analysis

Metal salts	**Chemical formula**	**Observations**	**Crystalline**	**IR**	**TGA**
Lanthanum (III) nitrate hydrate	$La(NO_3)_3{\cdot}6H_2O$	white precipitate	Yes	Yes	No
Indium (III) Chloride	$InCl_3$	white precipitate	Yes	No	No

5.6 IR results

The IR peaks apparent in Figures 5.3-5.6 is 2900 cm^{-1},1490 cm^{-1}, 1400 cm^{-1} and 750 cm^{-1}. These peaks would match up to carboxylate ions which could be represented by acetate. The peaks at around 2900 cm^{-1} would then be assigned to $C-H$. The peak at 1490 cm^{-1} woud likely be CH_3 stretching while The 1400 cm^{-1} would correspond to $O-H$. The 750 cm^{-1} peak is indicative of benzene derivatives from the linker.[31]

The Figures 5.3-5.6 have been plotted with a IR measurement of the linker H_6cpb. In the linker, the most characteristic peaks of 3400 cm^{-1} from $O-H$, 1680 cm^{-1} from $C=O$ and 1270 cm^{-1} from $C-OH$ are all present from the carboxylic acid group. These peaks are not present in the sample measurements, this is believed to be due to the linker being fully deprotonated and that the samples had dried over several months resulting in evaporation of the acetic acid.

In Figure 5.7 the time elapsed between synthesis and IR measurement was only 24 hours, this show all the characteristic peaks of the H_6cpb linker. This is due to acetic acid still being present in the sample.

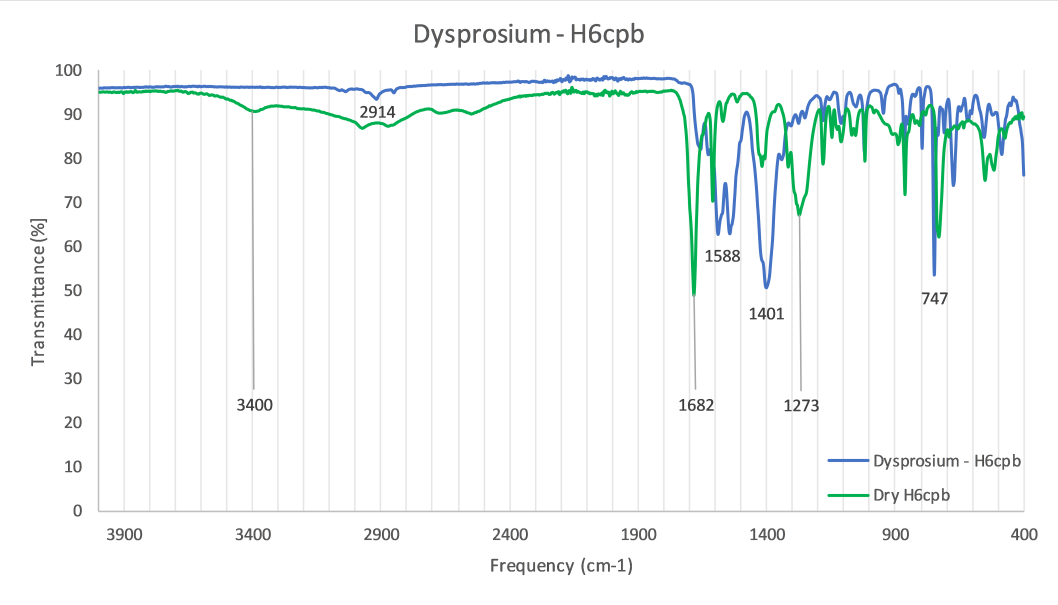


Figure 5.3: FTIR measurement using ATR of dysprosium sample with H_6cpb from synthesis in Section 4.2.

The data of 5.4 show very small peaks, the reason for this is believed to be due to the small sample available for testing. The only peaks which are clear would be 1403 cm^{-1} and 748 cm^{-1}.

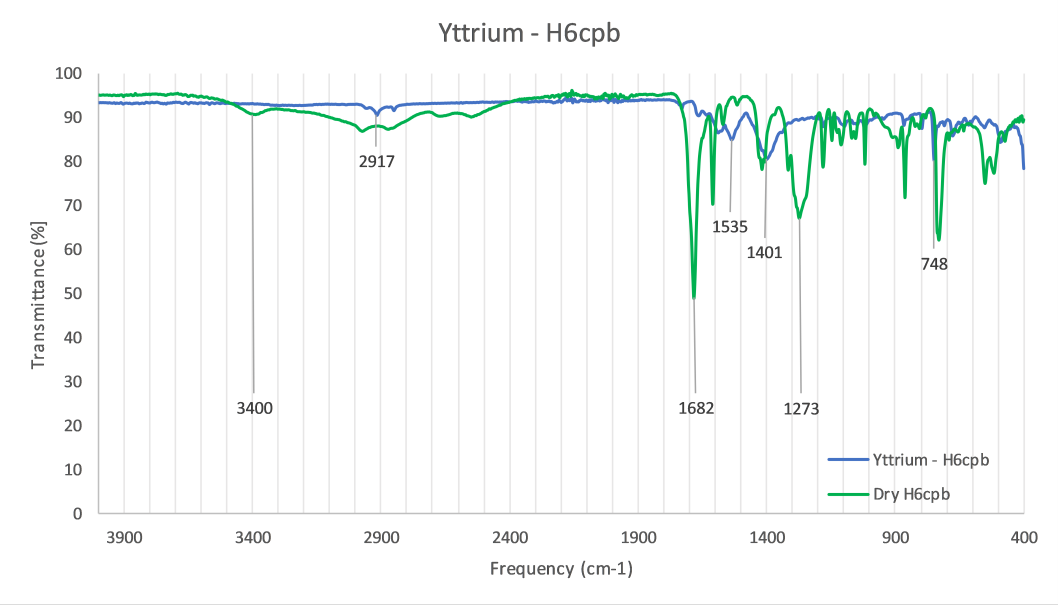


Figure 5.4: FTIR measurement using ATR of yttrium sample with H_6cpb from synthesis in Section 4.2.

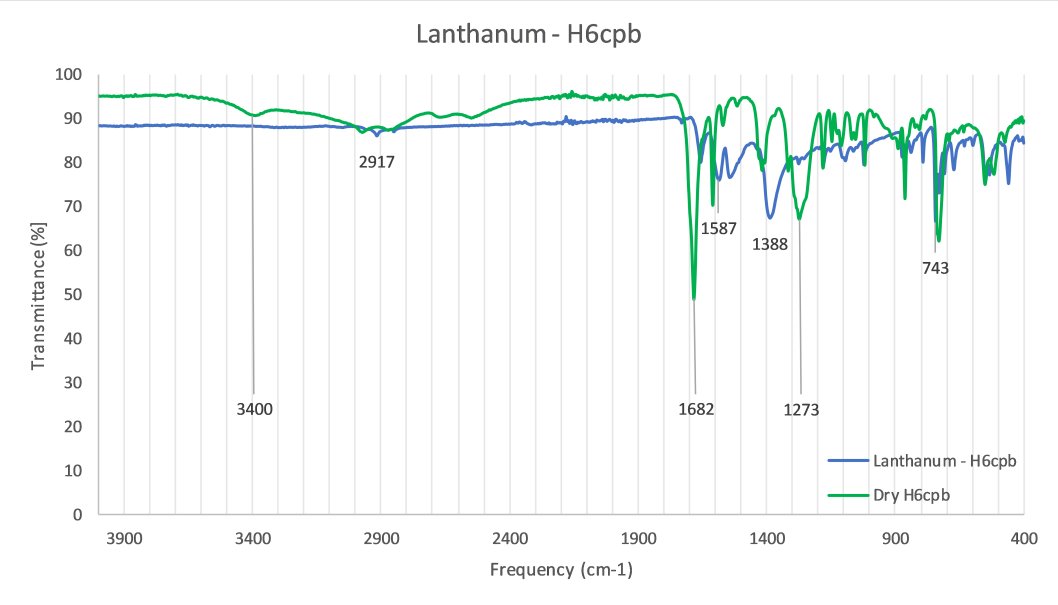


Figure 5.5: FTIR measurement using ATR of lanthanum sample with H_6cpb from synthesis in Section 4.2.

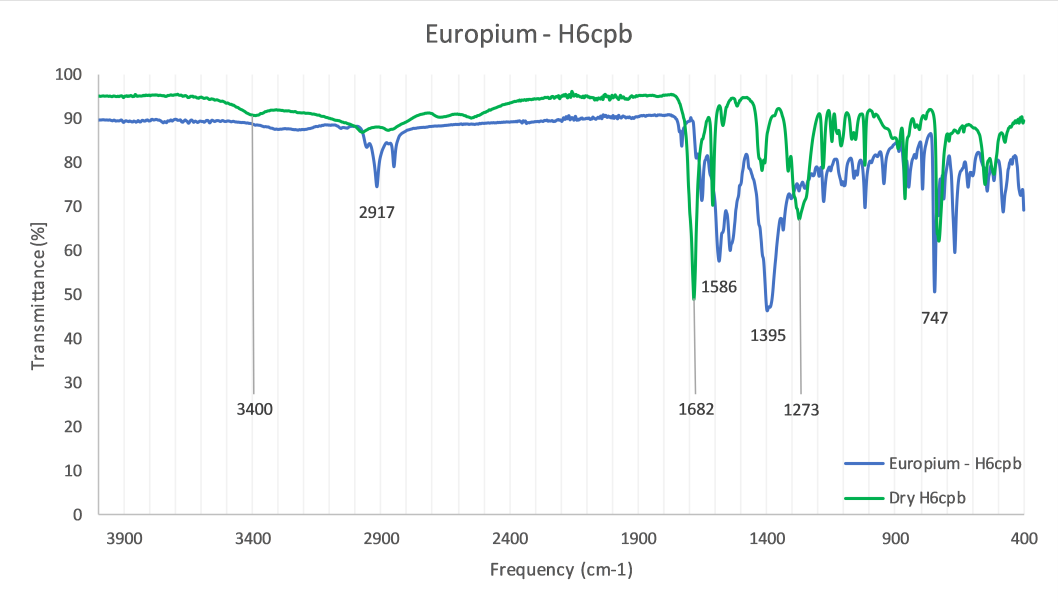


Figure 5.6: FTIR measurement using ATR of europium sample with H_6cpb from synthesis in Section 4.2.

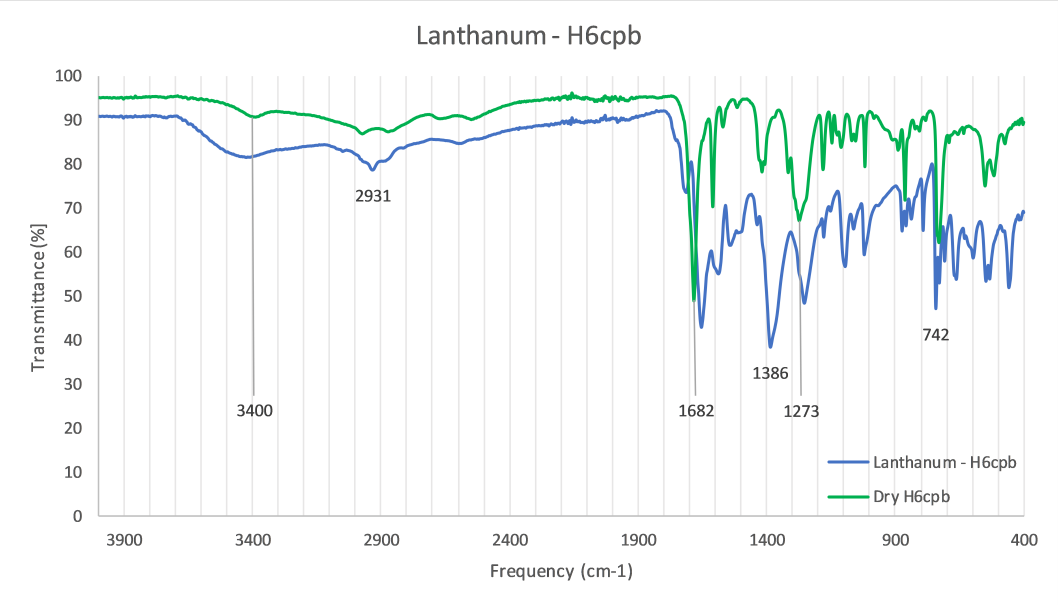


Figure 5.7: FTIR measurement using ATR of lanthanum sample with H_6cpb from synthesis in Section 4.5.

5.7 TGA results

Because of the small sample size, samples were not large enough to run all methods of analysis, in fact only dysprosium produced enough sample from synthesis to run in TGA. In Figure 5.8 the solvent evaporation can be seen from 127°C-300°C. At 407°C the thermal degradation of the MOF begins and lasts to 478°C. As the weight of MOF used for the TGA started at 1.92 mg, the weight at each temperature can be found in Table 5.4. No molecular structure can be confirmed from this data. However, by comparing calculations of different MOF structures formed by this combination, the data from the sample show promise of being a MOF.

Table 5.4: Calculated weight and mole for the sample containing dysprosium and H_6cpb from synthesis in Section 4.2

Sample	**Starting amount** [mg]	**Amount at** $300°C$ [mg]	**Amount at** $478°C$ [mg]	**H6cpb** [mol]	**Dysprosium** [mol]
Dysprosium	1.98	1.56	0.58	$1.31 * 10^{-6}$	$1.36 * 10^{-6}$

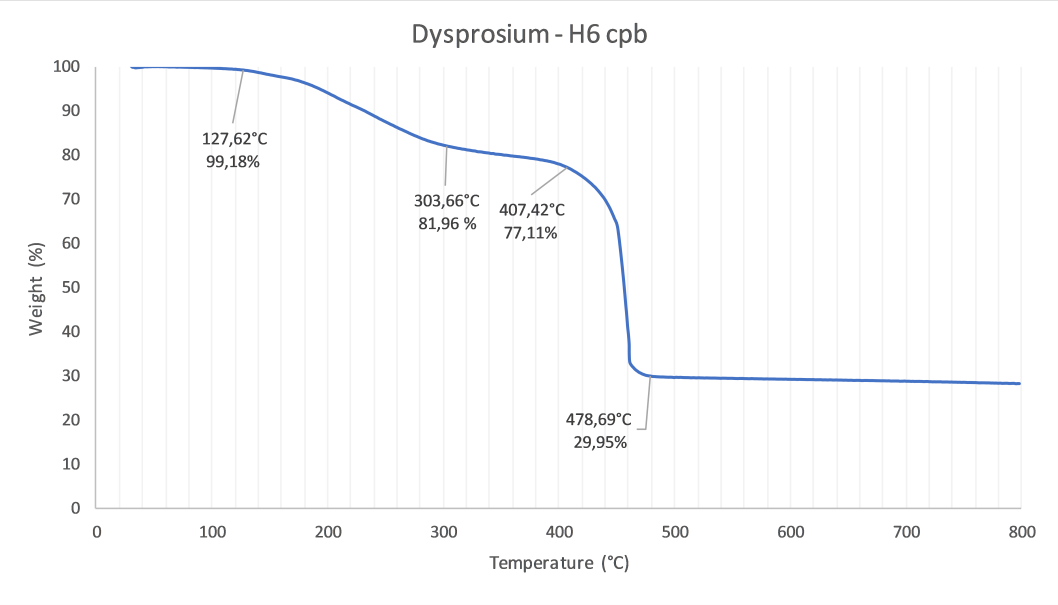


Figure 5.8: TGA data on dysprosium sample from synthesis in Section 4.2.

5.8 PXRD results

In Figure 5.9 the measurement of the indium MOF produced from synthesis in Section 4.5 can be seen. This synthesis was the only indium synthesis which produced precipitate. In Figure 5.9 the measurement has been plotted with a simulated powder diffraction pattern of MOF-894 which was produced by Nguyen et al.[18] As the plots match very accurately with each other it is likely that the MOF produced in this synthesis from indium is MOF-894.

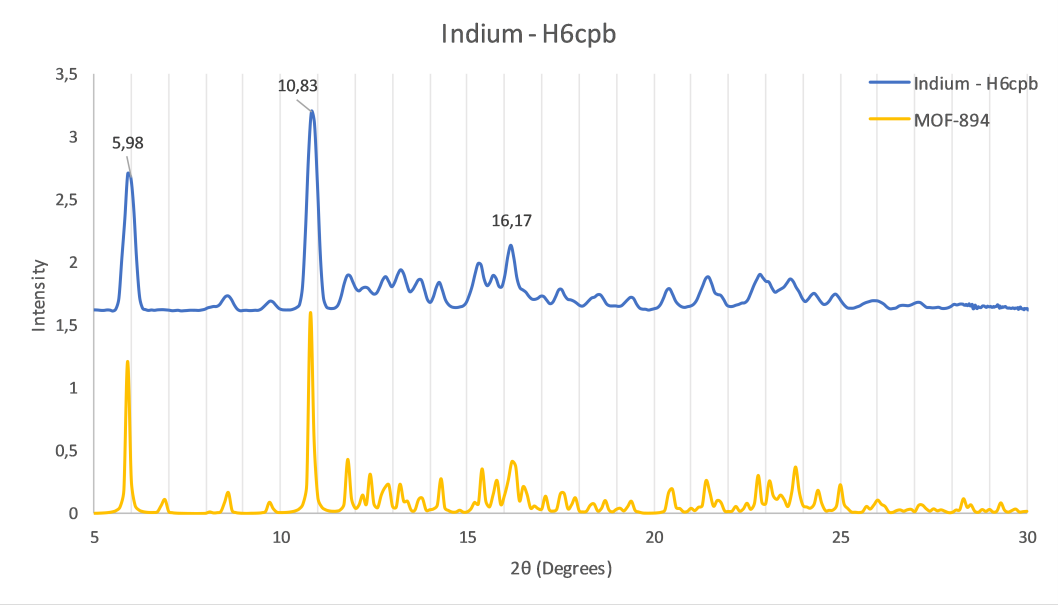


Figure 5.9: PXRD measurement of indium sample from synthesis in Section 4.5 in **blue**, this has been plotted with a simulated powder diffraction pattern of MOF-894 using Mercury in **orange.**

In Figures 5.11-5.10 a simulated powder pattern from MOF-889 by Nguyen et al.[10] has been plotted with the synthesized magnesium sample. By comparing the data, it can be

seen that the synthesized magnesium sample only slightly resemble the peaks of MOF-889. It cannot be completely ruled out that the sample can still be MOF-889 but the measurement may be slightly offset, or the sample may be heterogeneous resulting in smaller peaks in certain areas compared to simulated pattern. Further testing through SCXRD methods would be required to confirm this.

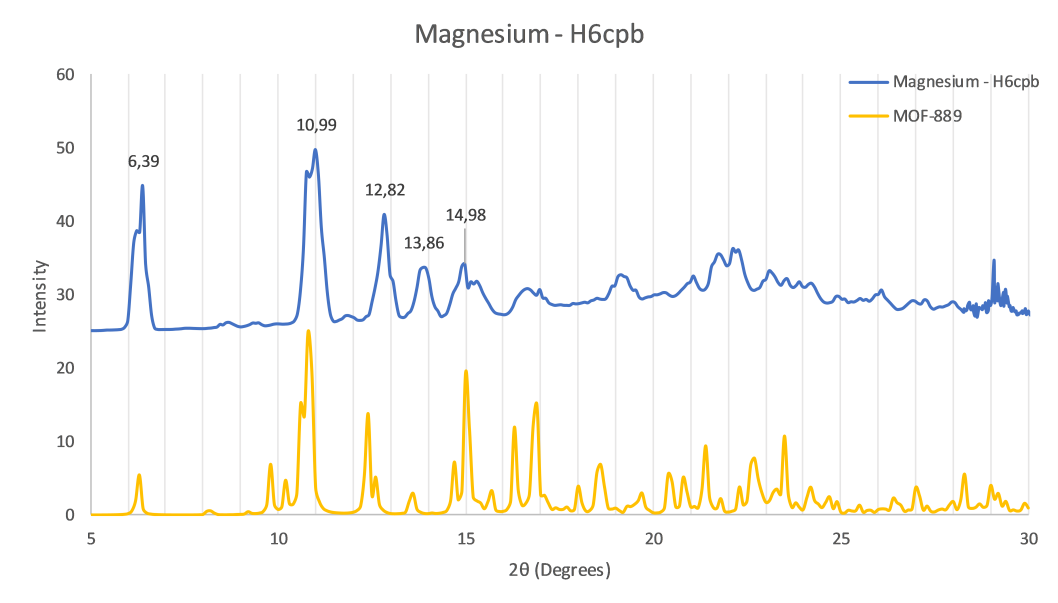


Figure 5.10: PXRD measurement of magnesium sample from synthesis in Section 4.1 in **blue**, this has been plotted with a simulated powder diffraction pattern of MOF-889 using Mercury in **orange**

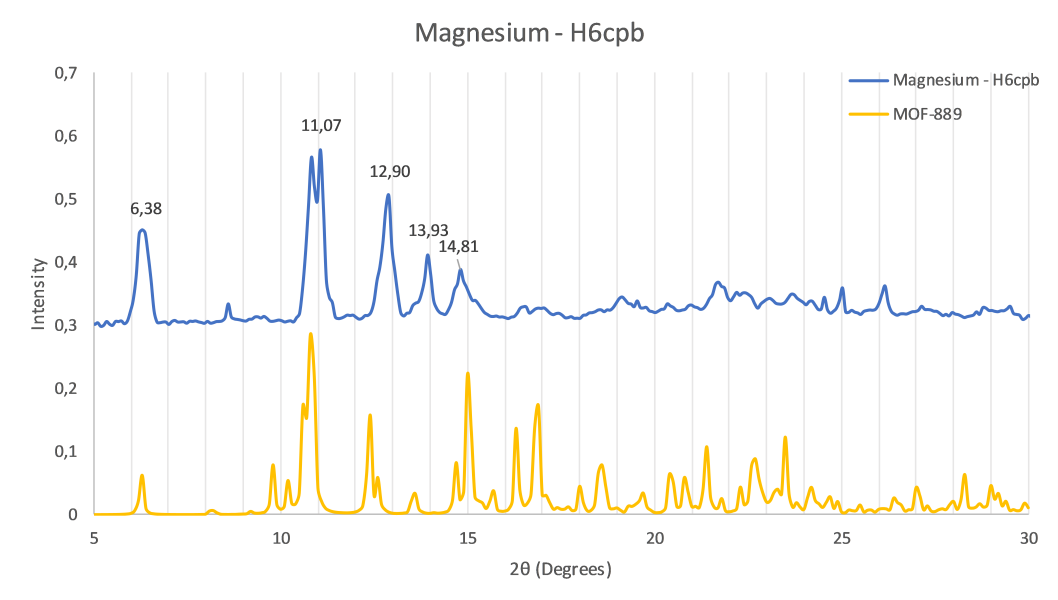


Figure 5.11: PXRD measurement of magnesium sample from synthesis in Section 4.2 in **blue**, this has been plotted with a simulated powder diffraction pattern of MOF-889 using Mercury in **orange**

A comparison between H_6cpb which has been crystallized in solution with dmf and H_6cpb without any other constituents can be seen in Figure 5.12. In this figure there are characteristic peaks for H_6cpb at the marked 2θ-angles. If the 2θ-angles at 16°or 17°is present in any data from the samples these could be identified as H_6cpb or H_6cpb crystallized

with solvent. The data for the H_6cpb crystallized with dmf has been previously measured through SCXRD and the PXRD pattern has been simulated through Mercury from unpublished results by Dr. Francoise Noa. The data for H_6cpb without any other constituent has been measured in the SAXS machine using the same method as previously stated.

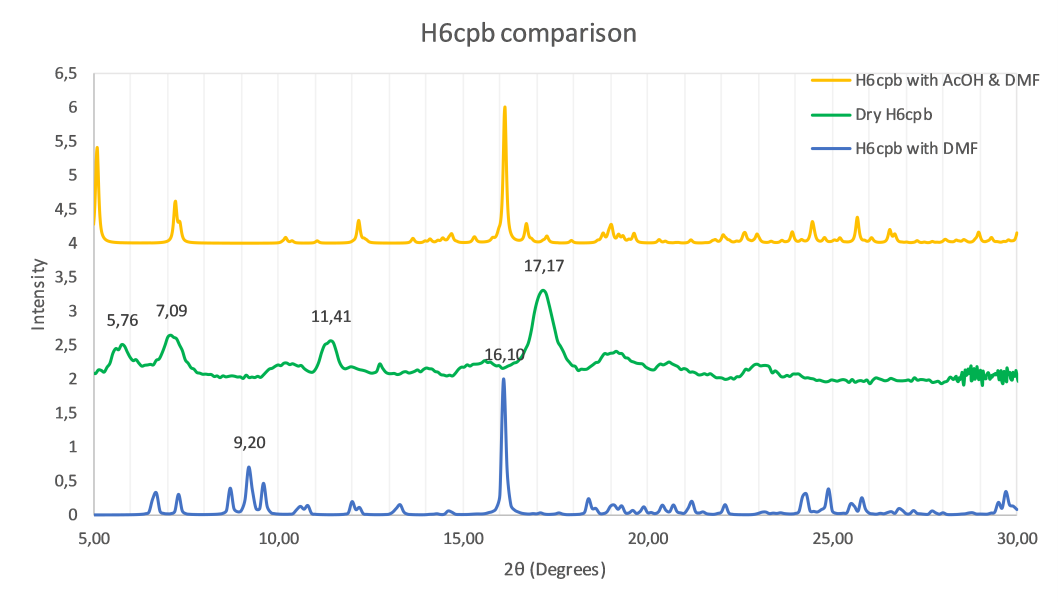


Figure 5.12: PXRD measurement of H_6cpb without any other constituents in **green** and simulated powder diffraction patterns of crystallized H_6cpb with dmf in **blue** and with H_6cpb with dmf and acetate in **yellow**.

In Figures 5.9-5.16 they all share similar 2θ-peaks around 6°and 11°. These peaks would match a lattice spacing of 14.3 Å and 8.3 Å respectively which can be calculated through Equation 2.1. The lattice parameter of 14.3 Å match the length across a H_6cpb molecule when measured in Mercury from SCXRD measurements done by Nguyen et al.[10,18] on MOF-894 and MOF-889. Images of this can be found in Appendix 2. This indicates that there is crystalline material which contains the linker but does not mean that the crystalline material would be a MOF. The source of the 8.3 Å lattice parameter has not been determined.

As the other metals have not been previously been used for synthesis of MOFs with H_6cpb there is no SCXRD measurement to compare with. However, the similarities in peak data may be the results of isostructural crystals which has been produced. Without the SCXRD measurement of the samples it cannot be concluded if these are MOFs or not. In Figures 5.13-5.17 the data has been compared to PXRD patterns seen Figure 5.12. By comparing the samples with this data, it is clear that the samples do not consist of unreacted H_6cpb as all the samples are missing the remarkable peak at 17°. The samples also do not consist of H_6cpb crystallized with dmf as the remarkable peak present at 16°is not present in the sample data.

It can also be deduced that lower angles of 2θ relates to a lattice spacing of 14.3 Å ($2\theta = 6°$) and 8.3 Å ($2\theta = 11°$). which would not be as high if there were unreacted metal salts in the sample. This concludes that a reaction has occurred between the metal salt and the linker, if a MOF has been formed cannot be deduced.

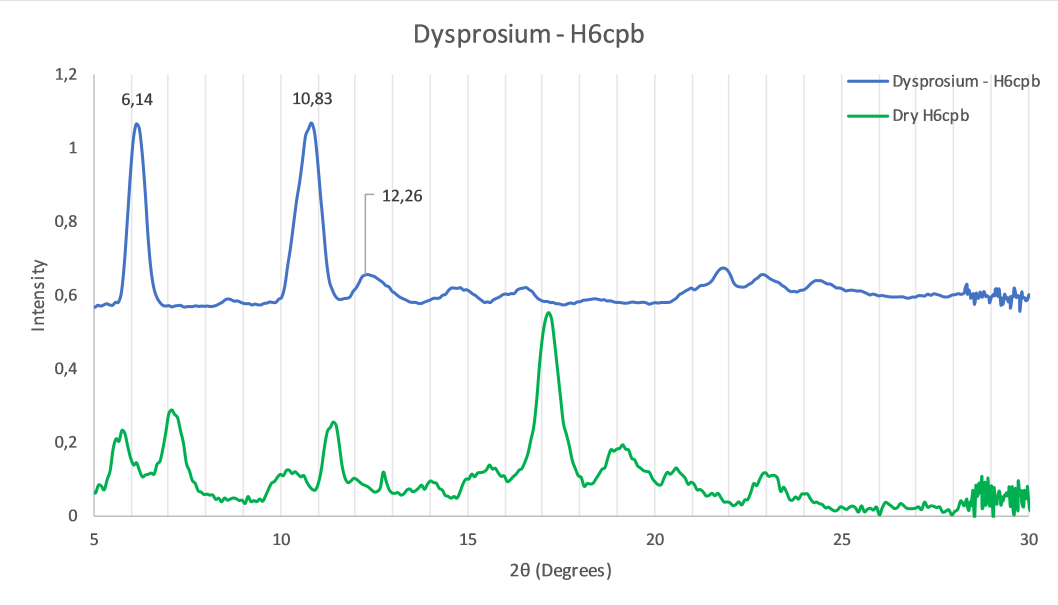


Figure 5.13: PXRD through SAXS measurement of dysprosium sample from synthesis in Section 4.2 in **blue**, this has been plotted with a diffraction pattern of H_6cpb without any constituents in **green**.

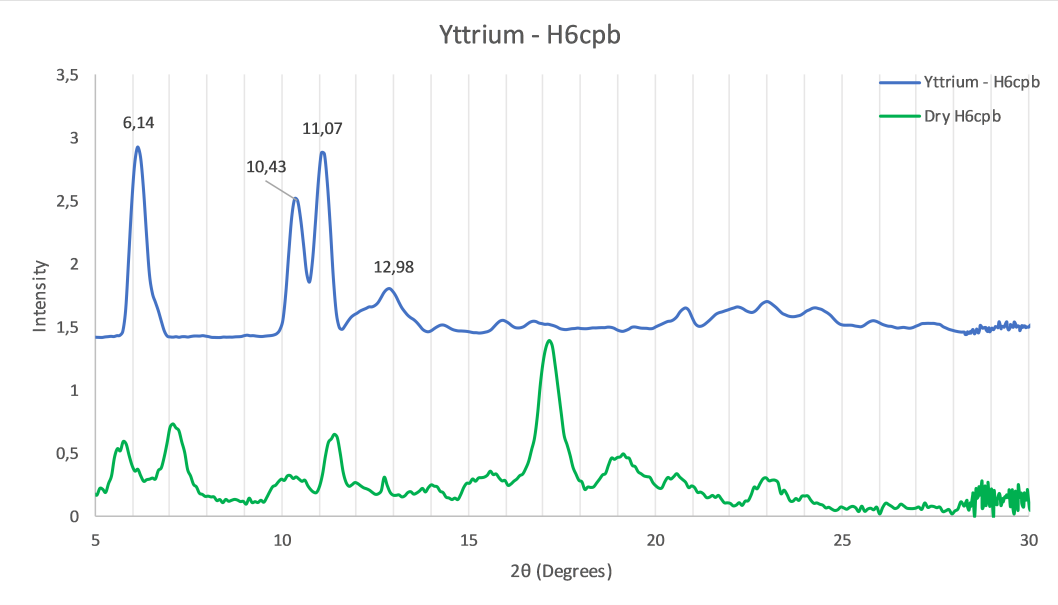


Figure 5.14: PXRD measurement of yttrium sample from synthesis in Section 4.2 in **blue**, this has been plotted with a diffraction pattern of H_6cpb without any constituents in **green**.

If Figure 5.15 and Figure 5.13 is compared it can be seen that the dysprosium and europium samples show very similar peak data both in size and placement. This is believed to be due to the similar chemistry of the lanthanide metals and the reaction for both samples is believed to be the same. This would mean that the precipitate for these samples should be isostructural.

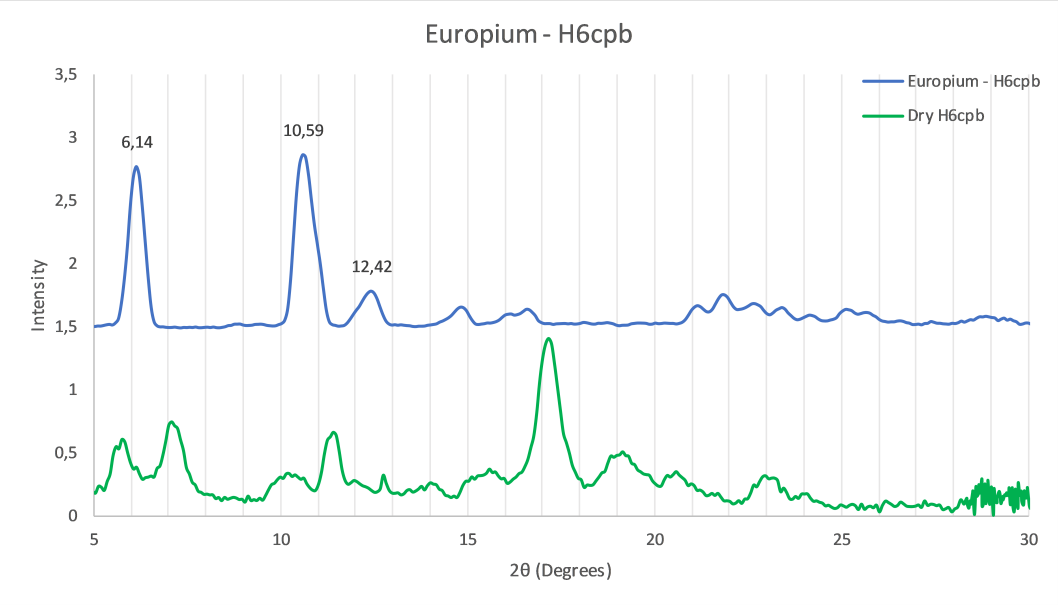


Figure 5.15: PXRD measurement of europium sample from synthesis in Section 4.2 in **blue**, this has been plotted with a diffraction pattern of H_6cpb without any constituents in **green**.

The lanthanum sample seen in Figure 5.16 show interesting results because of the clear peaks which can be seen both at lower and higher 2θ. This could be an indication that a more homogeneous crystal has formed. As seen in comparisons with MOF-889 and MOF-894 there should be peak data at higher 2θ values.

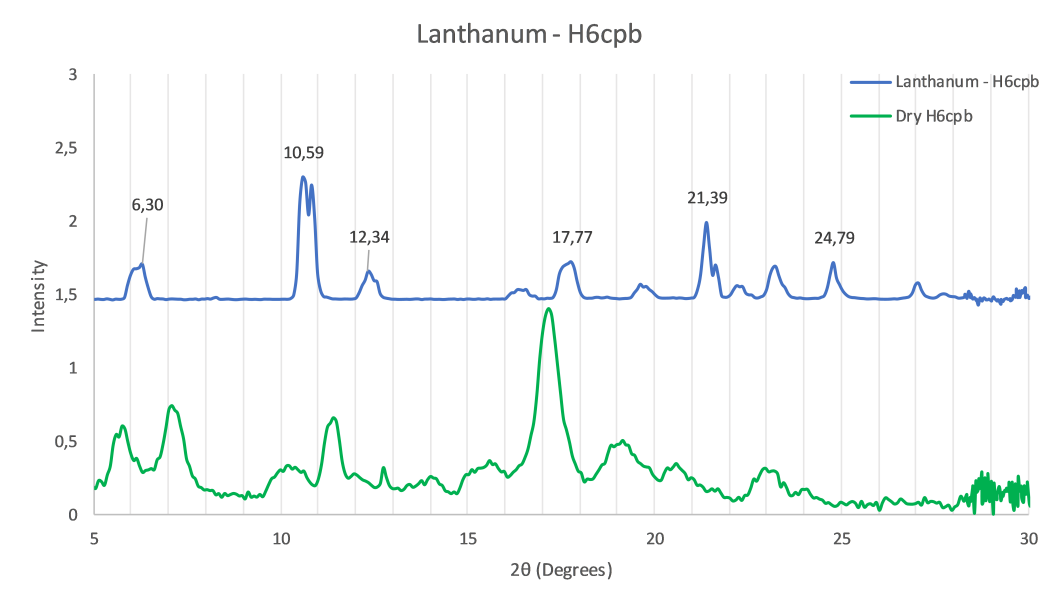


Figure 5.16: PXRD through SAXS measurement of lanthanum sample from synthesis in Section 4.2 in **blue**, this has been plotted with a diffraction pattern of H_6cpb without any constituents in **green**.

Figure 5.17 is the scaled up synthesis of lanthanum with H_6cpb, if compared with 5.16 all the same peaks are present in both graphs. The data has very clear peaks and with a clear interval, this is indicative of a crystal structures where the peaks represent lattice planes. Which is promising results for the sample to be a MOF.

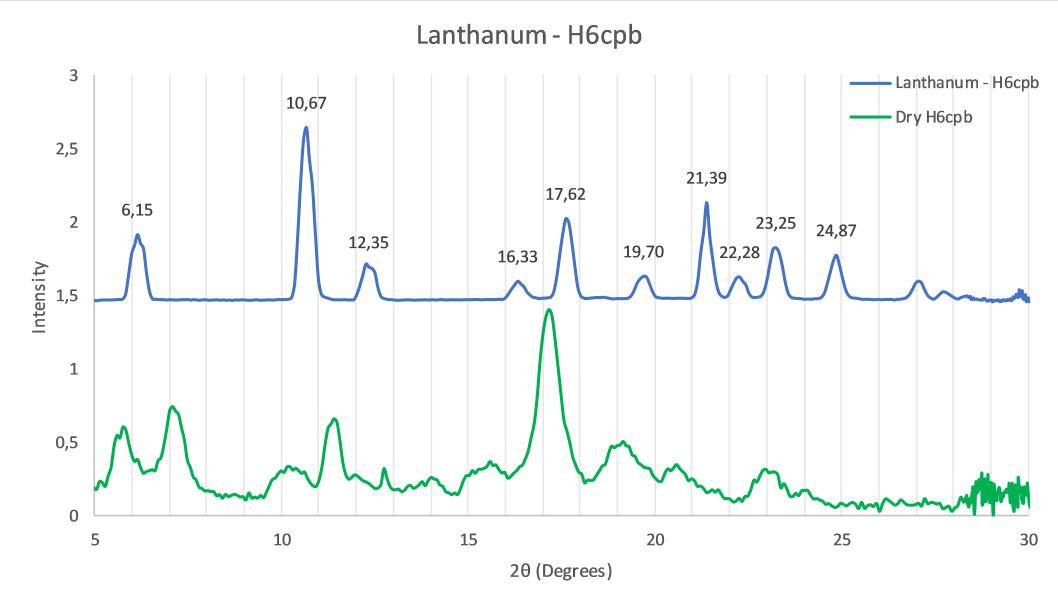


Figure 5.17: PXRD through SAXS measurement of lanthanum sample from synthesis in Section 4.5 in **blue**, this has been plotted with a diffraction pattern of H_6cpb without any constituents in **green**.

5.9 UV-test

A UV-light test was only if interest for europium samples. Europium +3 ions have very clear light absorption peaks which results in fluorescence. By shining a UV-light of both 254 nm and 302 nm the red-light fluorescence of europium can be seen. This would confirm that the crystals are containing europium and are not only made of the H_6cpb linker. This can be seen in Figures 5.18-5.19.

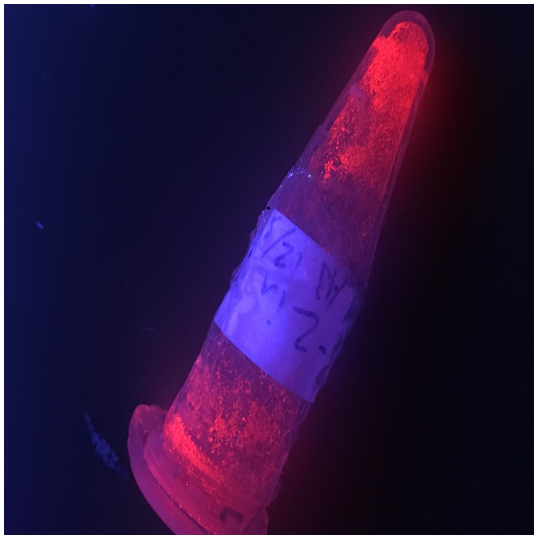


Figure 5.18: A fluorescent red light emitted by the europium sample from synthesis in Section. 4.2 when shining a 254 nm UV-light on the europium sample.

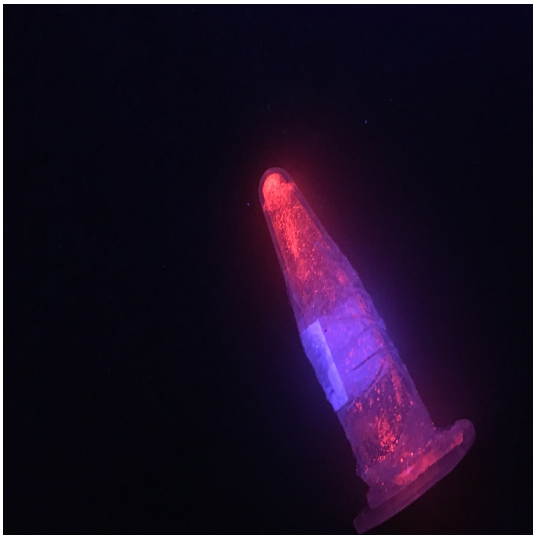


Figure 5.19: A fluorescent red light emitted by the europium sample from synthesis in Section. 4.2 shining a 302 nm UV-light on the europium sample.

Lanthanum, dysprosium and yttrium samples were also tested under UV-light. However, these metal ions do not have absorption peaks in these wavelengths and there is no luminescent properties in the linker. It was done to assess if the crystals would gain any other absorption peaks when bonded to the linker, but this was not the case.

5.10 TEM results

A preliminary structure determination of the lanthanum sample made in Section 4.5 could be solved through TEM analysis. The resulting structure in Figure 5.20 would be that of a rod MOF which is the type of MOF that has a 1-periodic metal SBU. This type of SBU lines up to a "rod" which is illustrated in Figures 5.21-5.22. The crystalline structure could be confirmed to be of the space group P/6 2 2 which is a chiral space group with the suggested chemical structure [La(cpb)$(dma)_3$] and the new MOF will be called CTH-17. The counterions in the structure is dimethylacetamide (dma) cations, which are formed during synthesis from dmf in the presence of acid.

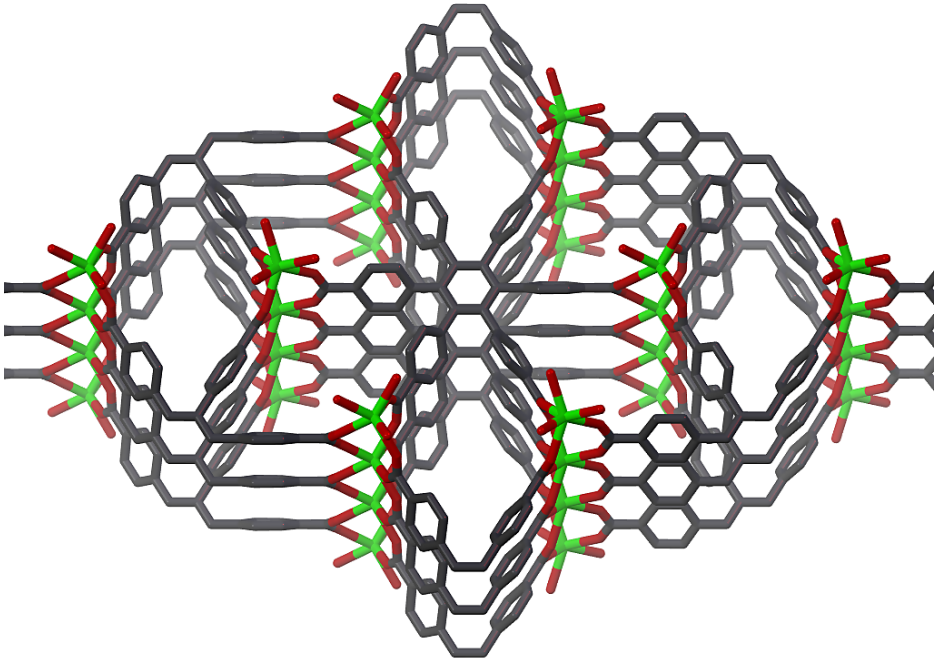


Figure 5.20: A preliminary structure of CTH-17 without the counterions. Where **green** is lanthanum, **red** is oxygen and **grey** is carbon.

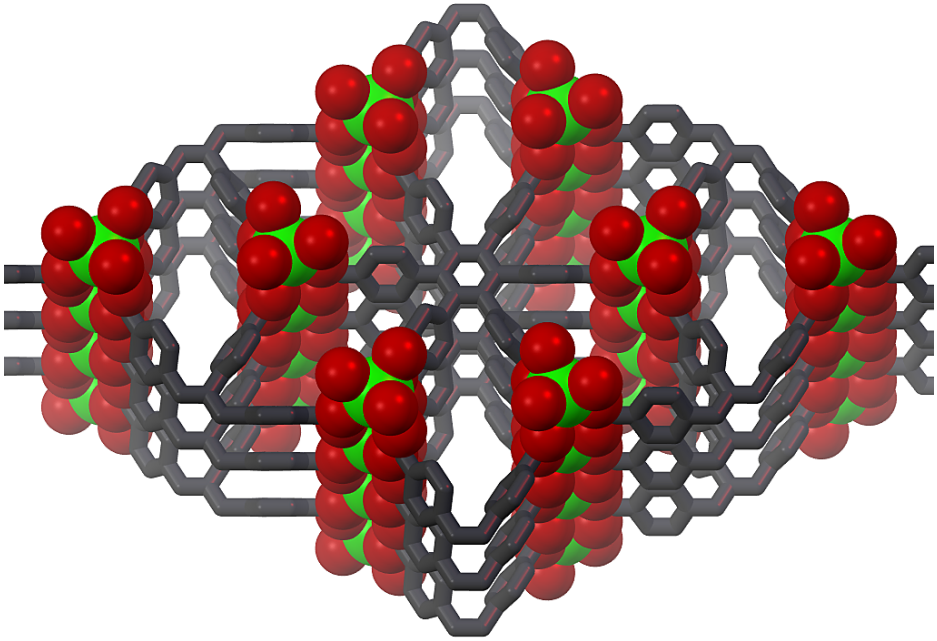


Figure 5.21: A preliminary structure of CTH-17 which illustrates the metal nodes as "rods". Where **green** is lanthanum, **red** is oxygen and **grey** is carbon.

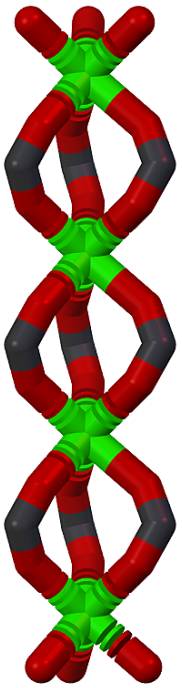


Figure 5.22: The SBU of the metal nodes in CTH-17, Where **green** is lanthanum, **red** is oxygen and **grey** is carbon.

6
Conclusion

The solvothermal synthesis has been successful of producing MOFs, this can be confirmed by the comparison of MOF-894 and the indium sample produced. It also shows that to produce MOFs of certain species an autoclave would be required to produce a completely sealed environment for the reaction to occur.

Autoclave synthesis was primarily used for metal species which would not produce precipitate in the microwave vials. It proved successful in the case of indium. However, this has not always been successful and attempts of synthesis with chromium MOFs in both microwave vials and autoclaves has not resulted in precipitate. This is believed due to there still being oxygen present which prevents reactions between the linkers and the metal.

Even though testing through SCXRD has not been available, XRD data from the formed crystals show a crystalline material produced through solvothermal synthesis which contains H_6cpb and is likely bonded to a metal.

From solving the structure of the lanthanum sample, it can be confirmed that this structure is a newly formed MOF. This MOF has a chiral space group of P/6 2 2 and has been named CTH-17.

Due to the COVID-19 virus there has been no opportunity to test all the crystals formed during this project with SCXRD or TEM. This has limited the project due to there being no available means for detailed crystal structure analysis of the crystals which have been produced. Because of this there is no conclusive information to state that any of the samples are MOFs, with the exception of the lanthanum sample.

Bibliography

[1] Markus J. Kalmutzki, Nikita Hanikel, and Omar M. Yaghi. "Secondary building units as the turning point in the development of the reticular chemistry of MOFs". In: *Science Advances* 4.10 (Oct. 2018), eaat9180. ISSN: 23752548. DOI: 10.1126/sciadv.aat9180.

[2] "Reticular Chemistry—Construction, Properties, and Precision Reactions of Frameworks". In: *Journal of the American Chemical Society* 138.48 (Dec. 2016), pp. 15507–15509. ISSN: 0002-7863. DOI: 10.1021/jacs.6b11821.

[3] Cristian Gozalvez, Jose L Zafra, Akinori Saeki, Manuel Melle-Franco, Juan Casado, and Aurelio Mateo-Alonso. "Charge transport modulation in pseudorotaxane 1D stacks of acene and azaacene derivatives". In: *Chem. Sci.* 10.9 (2019), pp. 2743–2749. DOI: 10.1039/C8SC04845B.

[4] Chu-Chen Chueh, Chih-I Chen, Yu-An Su, Hannelore Konnerth, Yu-Juan Gu, Chung-Wei Kung, and Kevin C.-W. Wu. "Harnessing MOF materials in photovoltaic devices: recent advances{,} challenges{,} and perspectives". In: *J. Mater. Chem. A* 7.29 (2019), pp. 17079–17095. DOI: 10.1039/C9TA03595H.

[5] Omar M Yaghi, Michael O'Keeffe, Nathan W Ockwig, Hee K Chae, Mohamed Eddaoudi, and Jaheon Kim. "Reticular synthesis and the design of new materials". In: *Nature* 423.6941 (2003), pp. 705–714. ISSN: 1476-4687. DOI: 10.1038/nature01650.

[6] Bunyarat Rungtaweevoranit, Christian S Diercks, Markus J Kalmutzki, and Omar M Yaghi. "Spiers Memorial Lecture: Progress and prospects of reticular chemistry". In: *Faraday Discuss.* 201.0 (2017), pp. 9–45. DOI: 10.1039/C7FD00160F.

[7] Ioannis Spanopoulos, Constantinos Tsangarakis, Sarah Barnett, Harriot Nowell, Emmanuel Klontzas, George E Froudakis, and Pantelis N Trikalitis. "Directed assembly of a high surface area 2D metal–organic framework displaying the augmented "kagomé dual" (kgd-a) layered topology with high H2 and CO2 uptake". In: *Inorg. Chem. Front.* 4.5 (2017), pp. 825–832. DOI: 10.1039/C6QI00547K.

[8] Irena Senkovska and Stefan Kaskel. "Solvent-Induced Pore-Size Adjustment in the Metal-Organic Framework [Mg3(ndc)3(dmf)4] (ndc = naphthalenedicarboxylate)". In: *European Journal of Inorganic Chemistry* 2006.22 (Nov. 2006), pp. 4564–4569. ISSN: 1434-1948. DOI: 10.1002/ejic.200600635.

[9] David Britt, Hiroyasu Furukawa, Bo Wang, T Grant Glover, and Omar M Yaghi. "Highly efficient separation of carbon dioxide by a metal-organic framework replete with open metal sites". In: *Proceedings of the National Academy of Sciences* 106.49 (Dec. 2009), 20637 LP –20640. DOI: 10.1073/pnas.0909718106.

[10] Phuong T K Nguyen, Huong T D Nguyen, Hung Q Pham, Jaheon Kim, Kyle E Cordova, and Hiroyasu Furukawa. "Synthesis and Selective CO2 Capture Properties of a Series of Hexatopic Linker-Based Metal–Organic Frameworks". In: *Inorganic Chemistry* 54.20 (Oct. 2015), pp. 10065–10072. ISSN: 0020-1669. DOI: 10.1021/acs.inorgchem.5b01900.

[11] Jun-Hao Wang, Ying Zhang, Mian Li, Shu Yan, Dan Li, and Xian-Ming Zhang. "Solvent-Assisted Metal Metathesis: A Highly Efficient and Versatile Route towards Synthetically Demanding Chromium Metal–Organic Frameworks". In: *Angewandte Chemie International Edition* 56.23 (June 2017), pp. 6478–6482. ISSN: 1433-7851. DOI: 10.1002/anie.201701217.

[12] Michał K Leszczyński, Arkadiusz Kornowicz, Daniel Prochowicz, Iwona Justyniak, Krzysztof Noworyta, and Janusz Lewiński. "Straightforward Synthesis of Single-Crystalline and Redox-Active Cr(II)-carboxylate MOFs". In: *Inorganic Chemistry* 57.9 (May 2018), pp. 4803–4806. ISSN: 0020-1669. DOI: 10.1021/acs.inorgchem.8b00395.

[13] Norma Cecilia Martinez-Gomez, Huong N Vu, and Elizabeth Skovran. "Lanthanide Chemistry: From Coordination in Chemical Complexes Shaping Our Technology to Coordination in Enzymes Shaping Bacterial Metabolism". In: *Inorganic Chemistry* 55.20 (Oct. 2016), pp. 10083–10089. ISSN: 0020-1669. DOI: 10.1021/acs.inorgchem.6b00919.

[14] Pengda Yi, Hongliang Huang, Yaguang Peng, Dahuan Liu, and Chongli Zhong. "A series of europium-based metal organic frameworks with tuned intrinsic luminescence properties and detection capacities". In: *RSC Adv.* 6.113 (2016), pp. 111934–111941. DOI: 10.1039/C6RA23263A.

[15] Jun Luo, Bao Shu Liu, Cong Cao, and Feng Wei. "Neodymium(III) organic frameworks (Nd-MOF) as near infrared fluorescent probe for highly selectively sensing of Cu2+". In: *Inorganic Chemistry Communications* 76 (2017), pp. 18–21. ISSN: 1387-7003. DOI: https://doi.org/10.1016/j.inoche.2017.01.008.

[16] Sarah L Griffin, Claire Wilson, and Ross S Forgan. "Uncovering the Structural Diversity of Y(III) Naphthalene-2,6-Dicarboxylate MOFs Through Coordination Modulation". In: *Frontiers in Chemistry* 7 (2019), p. 36. ISSN: 2296-2646. DOI: 10.3389/fchem.2019.00036.

[17] Hala Atallah, Mahmoud ELcheikh Mahmoud, Abdinoor Jelle, Alan Lough, and Mohamad Hmadeh. "A highly stable indium based metal organic framework for efficient arsenic removal from water". In: *Dalton Trans.* 47.3 (2018), pp. 799–806. DOI: 10.1039/C7DT03705H.

[18] Phuong T K Nguyen, Huong T D Nguyen, Hung N Nguyen, Christopher A Trickett, Quang T Ton, Enrique Gutiérrez-Puebla, M Angeles Monge, Kyle E Cordova, and Felipe Gándara. "New Metal–Organic Frameworks for Chemical Fixation of CO2". In: *ACS Applied Materials & Interfaces* 10.1 (Jan. 2018), pp. 733–744. ISSN: 1944-8244. DOI: 10.1021/acsami.7b16163.

[19] Francoise M Amombo Noa, Erik Svensson Grape, Steffen M Brülls, Ocean Cheung, Per Malmberg, A Ken Inge, Christine J McKenzie, Jerker Mårtensson, and Lars Öhrström. "Metal–Organic Frameworks with Hexakis(4-carboxyphenyl)benzene: Extensions to Reticular Chemistry and Introducing Foldable Nets". In: *Journal of the American Chemical Society* (Apr. 2020). ISSN: 0002-7863. DOI: 10.1021/jacs.0c02984.

[20] Makoto Yoneya, Seiji Tsuzuki, and Masaru Aoyagi. "Simulation of metal–organic framework self-assembly". In: *Phys. Chem. Chem. Phys.* 17.14 (2015), pp. 8649–8652. DOI: 10.1039/C5CP00379B.

[21] Andrew D. Bond. "Single-Crystal X-ray Diffraction". In: *Analytical Techniques in the Pharmaceutical Sciences*. Ed. by Anette Müllertz, Yvonne Perrie, and Thomas Rades. New York, NY: Springer New York, 2016, pp. 315–337. ISBN: 978-1-4939-4029-5. DOI: 10.1007/978-1-4939-4029-5{_}9.

[22] Abi Munajad, Cahyo Subroto, and Suwarno. "Fourier transform infrared (FTIR) spectroscopy analysis of transformer paper in mineral oil-paper composite insulation under accelerated thermal aging". In: *Energies* 11.2 (Feb. 2018). ISSN: 19961073. DOI: 10.3390/en11020364.

[23] A W Coats and J P Redfern. "Thermogravimetric analysis. A review". In: *Analyst* 88.1053 (1963), pp. 906–924. DOI: 10.1039/AN9638800906.

[24] Steffen Dreger, Manuela Pfinder, Lara Christianson, Stefan K Lhachimi, and Hajo Zeeb. "The effects of iodine blocking following nuclear accidents on thyroid cancer, hypothyroidism, and benign thyroid nodules: design of a systematic review". eng. In: *Systematic reviews* 4 (Sept. 2015), p. 126. ISSN: 2046-4053. DOI: 10.1186/s13643-015-0106-3.

[25] Sumito Yoshida, Mayo Ojino, Takayoshi Ozaki, Takushi Hatanaka, Kaori Nomura, Masami Ishii, Kazuaki Koriyama, and Makoto Akashi. "Guidelines for iodine prophylaxis as a protective measure: information for physicians". eng. In: *Japan Medical Association journal : JMAJ* 57.3 (May 2014), pp. 113–123. ISSN: 1346-8650.

[26] Wei Xie, Di Cui, Shu-Ran Zhang, Yan-Hong Xu, and Dong-Lin Jiang. "Iodine capture in porous organic polymers and metal–organic frameworks materials". In: *Materials Horizons* 6.8 (2019), pp. 1571–1595. ISSN: 2051-6347. DOI: 10.1039/C8MH01656A.

[27] M Younas, M Sohail, L K Leong, M J K Bashir, and S Sumathi. "Feasibility of CO2 adsorption by solid adsorbents: a review on low-temperature systems". In: *International Journal of Environmental Science and Technology* 13.7 (2016), pp. 1839–1860. ISSN: 1735-2630. DOI: 10.1007/s13762-016-1008-1.

[28] Yuan-Biao Huang, Jun Liang, Xu-Sheng Wang, and Rong Cao. "Multifunctional metal–organic framework catalysts: synergistic catalysis and tandem reactions". In: *Chem. Soc. Rev.* 46.1 (2017), pp. 126–157. DOI: 10.1039/C6CS00250A.

[29] Lizhen Liu, Zizhu Yao, Yingxiang Ye, Chulong Liu, Quanjie Lin, Shimin Chen, Shengchang Xiang, and Zhangjing Zhang. "Enhancement of Intrinsic Proton Conductivity and Aniline Sensitivity by Introducing Dye Molecules into the MOF Channel". In: *ACS Applied Materials & Interfaces* 11.18 (May 2019), pp. 16490–16495. ISSN: 1944-8244. DOI: 10.1021/acsami.8b22327.

[30] Victor Engdahl. *Synthesis and development of metal-organic frameworks with focus on hexagon 3D topologies*. 2020.

[31] *Applications in Coordination Chemistry*. Wiley Online Books. Dec. 2008, p. 64. ISBN: 9780470405888. DOI: doi:10.1002/9780470405888.ch1.

Appendix 1

Images from synthesis

This section includes images which were taken in a Zeiss microscope of some of the samples that were synthesized.

Synthesis using hexatopic H_6cpb

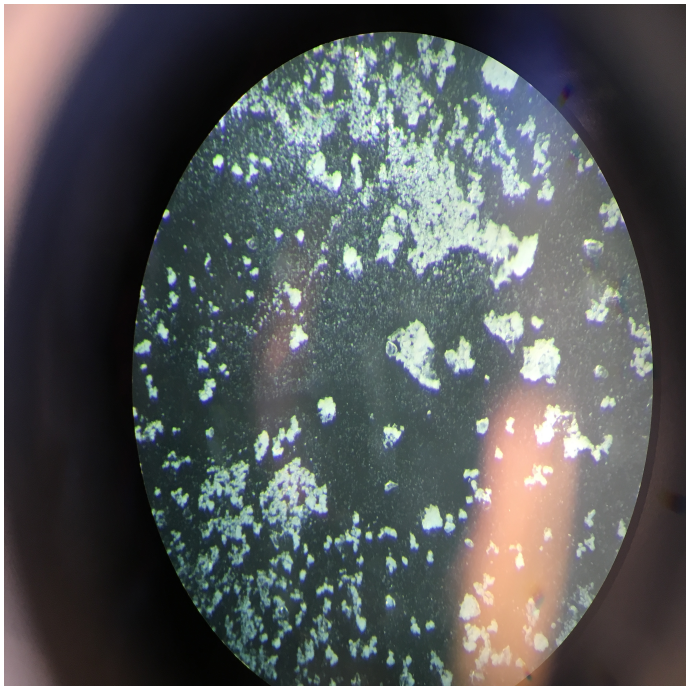


Figure 6.1: Europium percipitate from synthesis in Section 4.1.

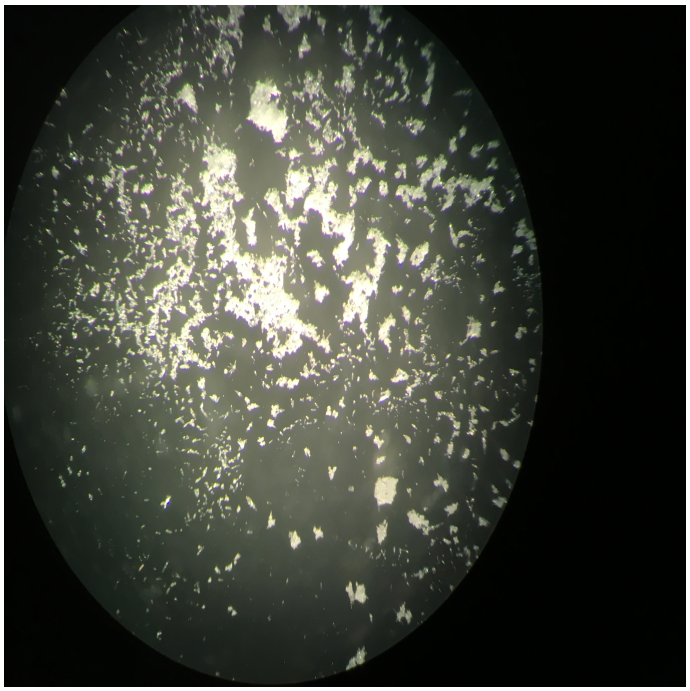


Figure 6.2: Lanthanum percipitate from synthesis in Section 4.1.

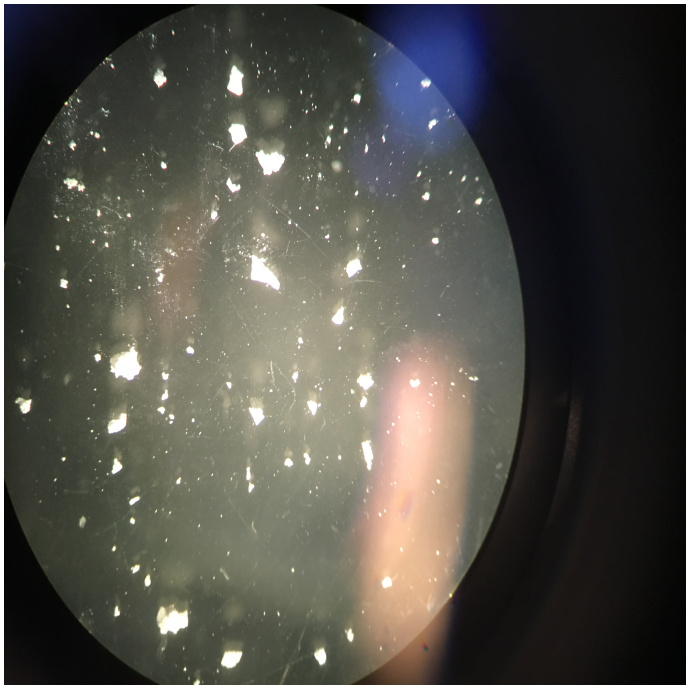


Figure 6.3: Magnesium precipitate using magnesium acetate from synthesis in Section 4.1.

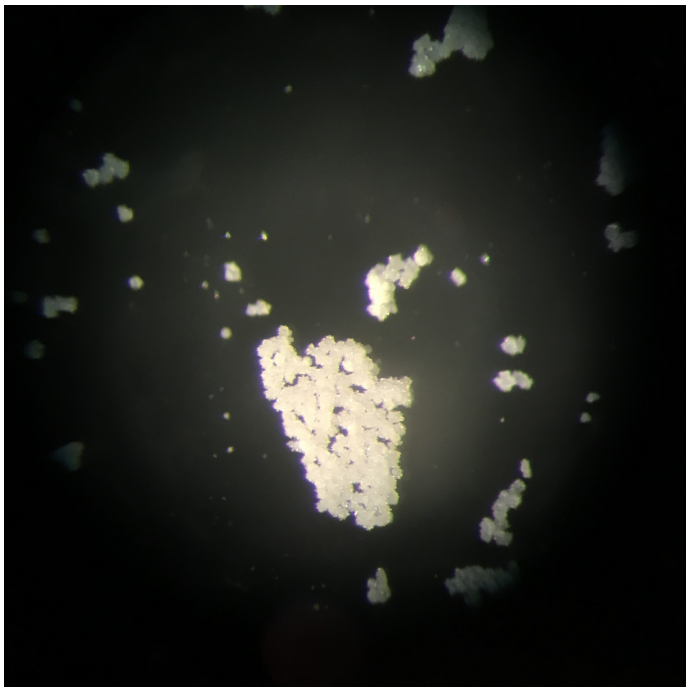


Figure 6.4: Magnesium precipitate using magnesium nitrate from synthesis in Section 4.1.

MOF-889 synthesis

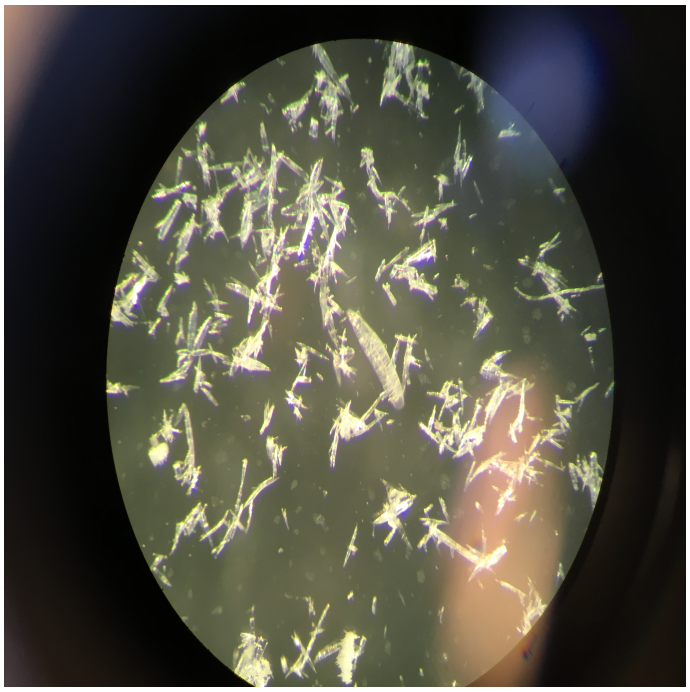


Figure 6.5: Magnesium precipitate from the MOF-889 synthesis

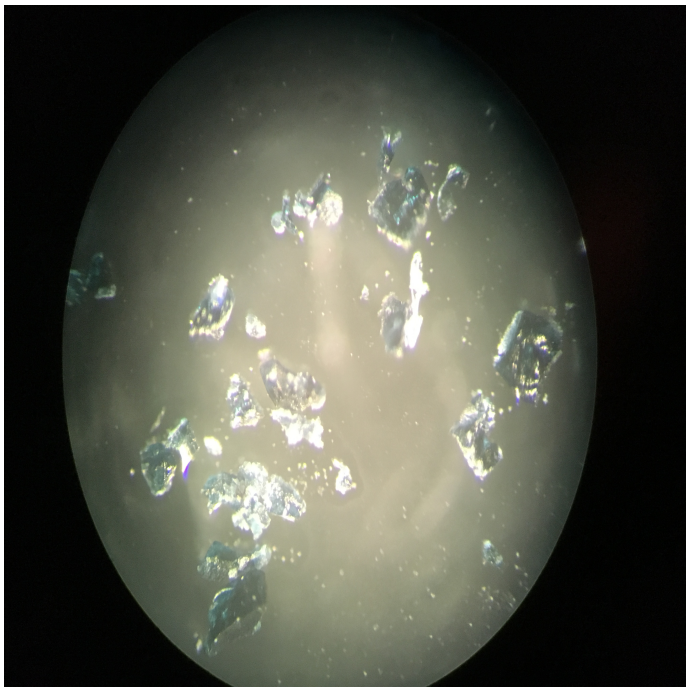


Figure 6.6: The chromium sample after drying the gel that had formed from synthesis in Section 4.3.

Lanthanum synthesis with H_6cpb

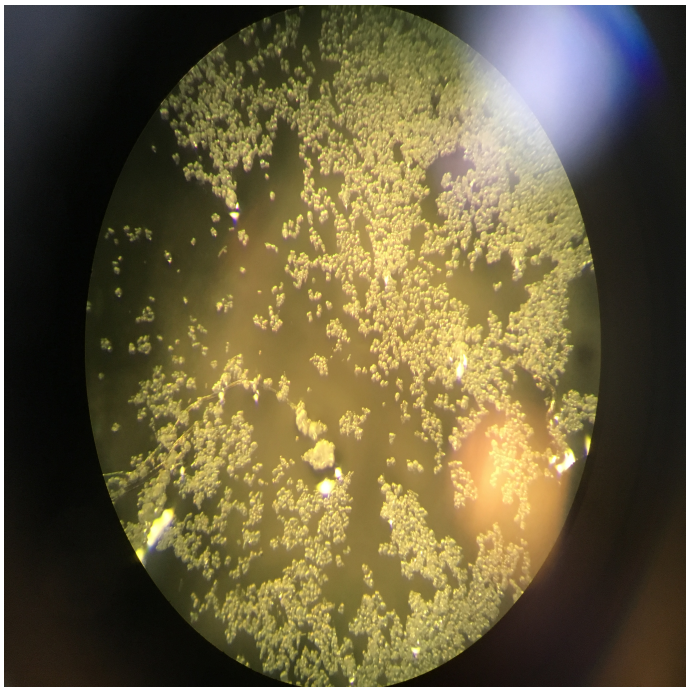


Figure 6.7: Lanthanum precipitate from synthesis in Section 4.5.

Appendix 2

This section includes images from Mercury where the measuring tool is used to determine the length of H_6cpb. The SCXRD measurements was of MOF-889 and MOF-894 was retrieved from reports by Nguyen et al.[10,18]

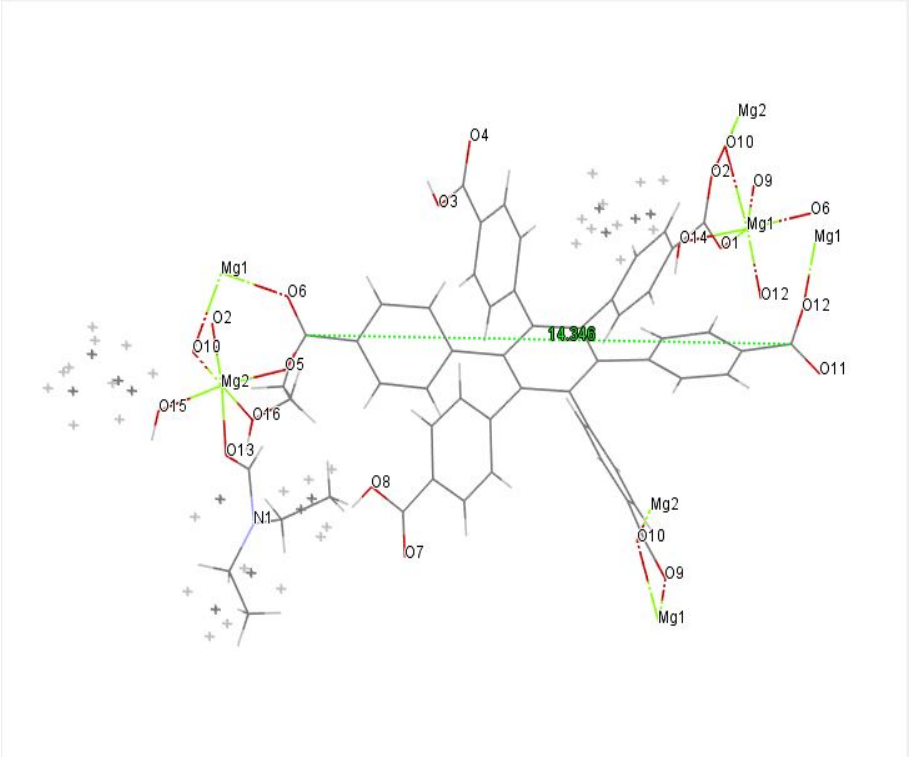


Figure 6.8: Magnesium MOF-889 simulated in Mercury program measuring the length of linker H_6cpb in the crystal to 14.3 Å.

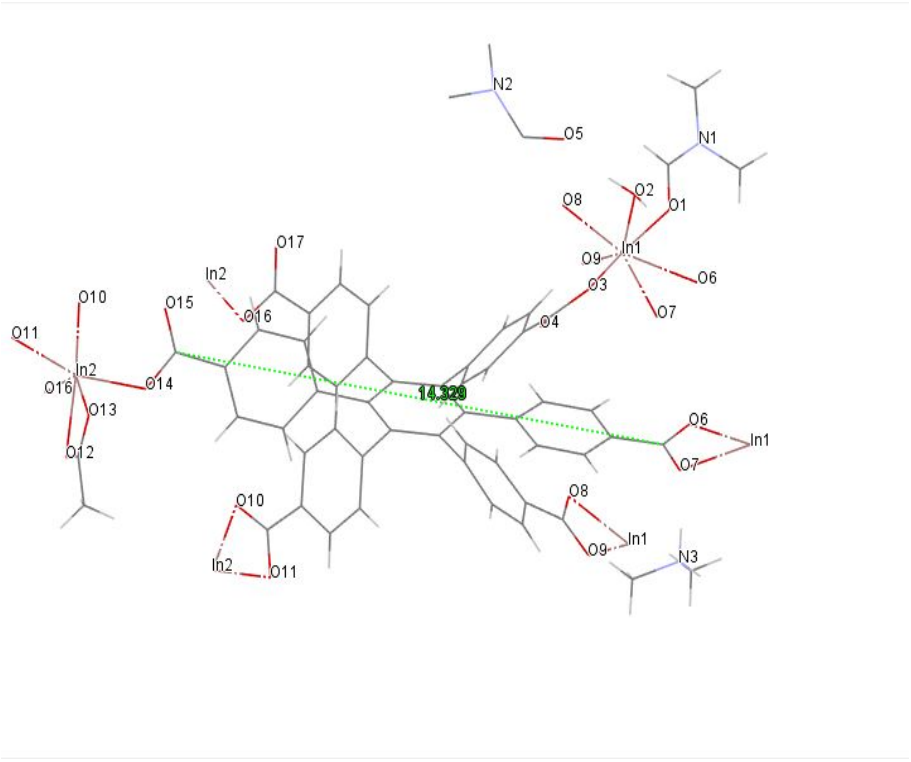


Figure 6.9: Magnesium MOF-894 simulated in Mercury program measuring the length of linker H_6cpb in the crystal to 14.3 Å.